The evolution of volcanic systems following sector collapse

Watt, Sebastian

DOI:
10.1016/j.jvolgeores.2019.05.012

The evolution of volcanic systems following sector collapse

Sebastian F.L. Watt
School of Geography, Earth and Environmental Sciences, University of Birmingham, Edgbaston, Birmingham B15 2TT, U.K.
e-mail: s.watt@bham.ac.uk
tel: 0121 414 6131

Abstract

Sector collapses affect volcanic edifices across all tectonic settings and involve a rapid redistribution of mass, comparable in scale to the largest magmatic eruptions. The eruptive behaviour of a volcano following sector collapse provides a test of theoretical relationships between surface loading and magma storage, which imply that collapse-driven unloading may lead to changes in eruption rate and erupted magma compositions. Large sector collapses are infrequent events globally, with all historical examples being relatively small in comparison to many of the events documented in the geological record. As a result, exploration of the impacts of sector collapse on eruptive behaviour requires detailed investigation of prehistoric collapses, but this is often hindered by poorly-resolved stratigraphic relationships and dating uncertainties. Nevertheless, observations from a number of volcanoes indicate sharp changes in activity following sector collapse. Here, a global synthesis of studies from individual volcanoes, in both arc and intraplate settings, is used to demonstrate a number of common processes in post-collapse volcanism. Multiple examples from large (>5 km^3) sector collapses in arc settings show that collapse may be followed by compositionally anomalous, large-volume and often effusive eruptions, interpreted to originate via disruption of a previously stable, upper-crustal reservoir. These anomalous eruptions highlight that magma compositions erupted during periods of typical (i.e. unperturbed by sector collapse) volcanism may not be representative of the range of compositions stored within a vertically extensive crustal reservoir. If eruptible magma is not present, upper-crustal reservoirs may rapidly solidify following collapse, without further eruption, allowing more mafic compositions to ascend to the surface with only limited upper-crustal modification, resulting in edifice regrowth at temporarily elevated eruption rates. Subsequent re-establishment of an upper-crustal reservoir further supports a relationship between surface loading and crustal storage, but long-term chemical and mineralogical differences between pre- and post-collapse evolved magmas imply that a newly-developed reservoir can overprint the influence of a preceding reservoir, forming a spatially and compositionally distinct plumbing system. These broad patterns are replicated in intraplate settings, despite differences in scale and melting processes; current evidence suggests that post-collapse evolution of intraplate volcanoes can be explained by unloading-induced destabilisation of the magma plumbing system, rather than increased melt production. What emerges from an apparently diverse set of observations is a systematic behaviour that strongly supports a coupling between edifice growth and magma ascent, storage and pressurisation. Eruption rates, erupted compositions, and the style of volcanism at any particular system may thus be modulated from the surface, and long-term shifts in surface behaviour may thus occur without any changes in the deep parts of magmatic systems. Observations of sharp post-collapse changes in erupted compositions, including the ascent of primitive mafic magmas, also require a crystal-dominated mid- to upper-crustal reservoir, consistent with recent models of crustal magmatic systems.

Keywords: sector collapse; magma storage; eruptive behaviour; edifice growth and destruction; debris avalanche

Highlights

- Global synthesis of volcano-magmatic evolution following sector collapse
- Decompression-driven reservoir disruption leads to anomalous post-collapse eruptions
- Rapid regrowth via mafic volcanism; subsequent re-establishment of shallow storage
- Implies direct modulation of shallow plumbing system development by surface load
- Common patterns in intraplate and arc settings

1. Introduction

Volcanic edifices across all tectonic settings are prone to structural instability and the generation of large landslides (Ui, 1983; Siebert, 1984), resulting in a redistribution of volcanic rock across the surrounding land surface. Landslides formed by edifice collapse span a wide range of dimensions, and their scars have been identified on volcanoes ranging from submerged seamounts to large ocean islands, and across subaerial composite volcanoes in both arc and intraplate settings (Siebert et al., 1987, 2006; Moore et al., 1989; Deplus et al., 2001; Coombs et al., 2007; Staudigel and Clague, 2010). The triggers for such landslides are varied. Although some, such as the sector collapse of Mount St Helen's in 1980, are directly associated with large magmatic eruptions (Glicken, 1996), structural failure is not always linked with magma ascent (Siebert et al., 1987; McGuire, 1996).

Historical observations and deposit characteristics suggest that structural failure of volcanic edifices generally occurs in a sudden, catastrophic event (although this may follow a long period of more gradual flank spreading (e.g., Moore et al., 1989; Neri et al., 2004; Wooller et al., 2004; Karstens et al., 2019); and failure itself may occur over several, shortly-spaced stages (Glicken, 1996; Hunt et al., 2013)). The base of the failure plane in large edifice collapses may lie deep within the volcano structure (Crandell, 1989; Glicken, 1996; Watt et al., 2014) and even intersect basement rock (e.g., Wadge et al., 1995; Shea et al., 2008), and in many cases cuts the central conduit. The mobilised mass may be remarkably large, in some cases accounting for >10% of the edifice volume. Sector collapses thus profoundly alter both the morphology of a volcano and the distribution of mass above an active magma plumbing system, potentially reducing the thickness of overlying rock by a kilometre or more.

Theoretical analyses suggest that mass redistribution following edifice collapse can influence pressurisation and failure conditions in stored magma bodies (Pinel and Jaupart, 2005; Pinel and Albino, 2013). It is therefore plausible that major collapses may be followed by changes in eruption rate or style, or in the composition of erupted magma. Anecdotal evidence from several individual volcanoes supports this idea (e.g., Tibaldi, 2004; Hora et al., 2009; Manconi et al., 2009), but it is not clear that there is a common pattern to post-collapse activity. In addition, some volcanoes show no apparent change in behaviour following large-scale edifice failure (e.g., Ponomareva et al., 2006; Zernack et al., 2012). Given the diversity of volcanic systems affected by edifice collapse, this is perhaps unsurprising, but the limited current understanding of the impacts of sector collapse on volcano-magmatic processes provides the motivation for this work. This paper draws on existing data on volcanoes affected by large-scale sector collapse to assess evidence for changes in subsequent volcanic activity, how this varies between volcano-tectonic settings, and whether any common processes or patterns of behaviour can be deduced.

2. Volcano sector collapse

The focus of this paper is on the impact that major volcanic structural failure has on the associated magmatic system, rather than on the mechanisms of the failure itself or of the mass-movement that it generates. Some brief terminological definitions are nevertheless necessary, given the range of terms used in published literature to describe volcanic collapses and their resultant deposits.

2.1. Terminology

All of the events documented in this paper involve the rapid gravity-driven transport of material away from a volcanic edifice, in a process that is effectively instantaneous relative to the timescale of volcano growth. The term sector collapse is used to describe the structural failure itself. Early uses of this term were used principally to describe major structural failures of composite arc volcanoes, where failed sectors of the cone generally encompassed the central conduit and summit of the volcano (e.g., Ui, 1983; Siebert, 1984; Siebert et al., 1987), providing a useful distinction from smaller mass movements that affect a single flank but don't extend to the central vent, which may be termed flank collapses. The term lateral collapse is also widely used, and emphasises the transport of mass away from the volcano, in contrast with the subsidence that accompanies caldera formation.

In general, sector collapses on polygenetic volcanoes result from large (as a proportion of the entire edifice) and deep-seated instabilities (Fig. 1), whereas some flank collapses are relatively superficial landslides, and not of interest here due to their small dimensions. The term sector collapse is thus used to emphasise that the studied events are large in the context of the parent edifice, and a minimum primary volume criterion of 1 km^3 is applied here. This value is somewhat arbitrary (and volumes of prehistoric events are often poorly constrained), but this limits the events under consideration to those that are at least equivalent in volume to a large magnitude (i.e. Magnitude >5; cf. Pyle, 2000) magmatic eruption.

Landslides on intraplate ocean islands form some of the largest mass-movements on Earth (Moore et al., 1989; Masson et al., 2002), potentially exceeding hundreds of cubic kilometres and dwarfing those on arc volcanoes (Fig. 1). The tectonic setting and magma generation process at these long-lived volcanic systems leads to islands that are morphologically very different to arc stratovolcanoes. Ocean islands typically have a lower overall gradient than arc volcanoes, and may be dominated by rift zones (Carracedo, 1994; Walter et al., 2005), potentially without a well-developed central magma system. Rift zone instabilities may be deeply rooted and lead to large flank landslides (not strictly meeting the sector collapse definition above), which nevertheless involve a smaller proportion of the total volcanic (i.e.

island) volume than many sector collapses in arc settings (Watt et al., 2014), despite their extreme size (Fig. 2). Such mass movements clearly have the potential to form a significant local stress perturbation, and are therefore considered here alongside their counterparts on composite arc volcanoes.

The term debris avalanche is widely used to describe volcanic landslides (and their resultant deposits) that involve non-juvenile material. However, the style of landslide movement can vary widely during transport (Scott et al., 2001) (and may involve failure over several discrete stages, particularly in ocean-island settings; cf. Hunt et al., 2013) and is also dependent on the nature of the failed mass, resulting in a wide range of deposit morphologies (Shea et al., 2008; Dufresne and Davies, 2009). The products of small volcanic landslides can also form block-rich debris avalanches (e.g. Voight and Sousa, 1994; Voight et al., 2002; Belousov et al., 2010), and at some volcanoes these may occur repeatedly on timescales as short as a few hundred years (e.g. Begét and Kienle, 1992). The term thus has no overall implications in terms of landslide volume or frequency.

2.2. Causal mechanisms

Ultimately, sector collapses are driven by gravitational instabilities arising from the geologically rapid construction of relatively steep topography, but are also influenced by internal structural and lithological heterogeneities (including basal discontinuities and spreading; van Wyk de Vries et al., 2001; Shea et al., 2008), alteration (Reid et al., 2001) and changes in pore-fluid pressure (Day, 1996), magmatic activity (Siebert et al., 1987), and external destabilising processes such as the retreat of glacial ice (Watt et al., 2009a; Tormey, 2010) or, possibly, sea level changes (cf. McMurtry et al., 2004; Hunt et al., 2014; Coussens et al., 2016; Paris et al., 2018). The precise trigger of sector collapses is generally difficult to identify, and may not be attributable to a single process. However, many sector collapses are not necessarily driven by magma ascent. Although some events, such as that at Mount St Helens in 1980, are a direct consequence of shallow intrusive or eruptive processes destabilising edifice flanks (Siebert et al., 1987), the role of eruptive activity in collapse is ambiguous in many other cases, even when sector collapses occur during a period of eruption (such as the 2018 collapse of Anak Krakatau, Indonesia). Other collapses show no evidence of associated magmatic activity, and examples such as the 1888 collapse of Bandai, Japan, which hasn't had a magmatic eruption since 25 ka (Yamamoto et al., 1999), suggest that sector collapses can occur entirely as a result of other destabilising processes. This is significant, because it implies that patterns of eruptive behaviour spanning sector collapses can provide a test of how magmatic systems respond to external stress changes, and how the changes in surface loading that accompany edifice growth influence crustal magmatic processes. For many prehistoric collapses, the role of magmatism in triggering sector collapse cannot be determined. Although the presence of juvenile material mixed within collapse deposits strongly suggests an eruption-driven process, the same is not true of juvenile products that immediately overlie collapse deposits, since they could reflect collapse-triggered eruption rather than the reverse. Such ambiguities in driving mechanisms and the contemporaneous state of the underlying magma reservoir present a challenge in evaluating the general effects of sector collapses on crustal magmatic processes.

2.3. Global distribution

Many individual sector collapses, and in particular their deposits, have been studied in detail (e.g. Wadge et al.,1995; Glicken, 1996; Shea et al., 2008; Hora et al., 2009). The majority of these well-studied examples are from subaerial arc volcanoes, although a significant number have also been documented from intraplate ocean islands such as Hawaii and the Canary Islands (Moore et al., 1989; Masson et al., 2002). Individual events are commonly recognised both from their hummocky deposits, which transport poorly-sorted and block-rich material tens of kilometres away from the volcano, and their characteristic amphitheatre-shaped scars (Siebert et al., 1987). The large number of identified examples indicates that collapse is a ubiquitous process affecting constructive volcanic landforms.

A global compilation of documented sector collapses, shown in Fig. 2, comprises over 300 events with estimated volumes >1 km^3, from over 200 individual volcanoes. Event volumes are often very poorly constrained, due to infilling or erosion of scars and limited information on deposit thicknesses. For events where specific volume estimates are available (Fig. 2), 71% are from subduction zone settings, 25% from intraplate ocean islands, and 4% from other settings. Compared to the global distribution of subaerial volcanoes (Global Volcanism Program, 2013), these values suggest that intraplate ocean-island landslides are over-represented in the dataset, since they account for 7% of volcanoes. Rift and continental intraplate volcanoes are under-represented, and there is also a slight under-representation of events in island-arc settings. These patterns are likely to reflect a sampling bias: the few regional-scale surveys of island arcs (Deplus et al., 2001; Coombs et al.. 2007; Silver et al.,

2009) show that sector collapse deposits occur around the majority of volcanic islands, but their identification is dependent on good quality bathymetric data. The over-representation of ocean-island collapses partly reflects the large number of events documented from Hawaii (Moore et al., 1989), the Canary Islands (Masson et al., 2002; 2006), the Cape Verde Islands (Masson et al., 2008) and Réunion (Oehler et al., 2008). It also reflects the long lifespan of many ocean islands and the large dimensions of their landslides, meaning that relatively ancient deposits can still be identified while those of a similar age in subduction-zone settings are more likely to have been buried, or their scars eroded.

In subduction zone settings, over 50% of documented sector collapses (only considering those >1 km^3 and with a specified volume) have volumes between one and five cubic kilometres, with a thick tail of larger events that extends up to 50 km^3 (Fig. 2). This pattern mirrors the overall size distribution of typical arc volcanoes: a compilation of 400 subaerial arc stratovolcanoes (Grosse et al., 2014) indicates a median edifice volume of 20.1 km^3 but a mean volume of 43 km^3, skewed by a small number of very large edifices that exceed 200 km^3 in volume. There are several examples of sector collapses that mobilise 10% of the total edifice volume, with some affecting over 25% of the total volcanic structure (e.g. Wadge et al., 1995; Zernack et al., 2012). Given typical lifetimes of 10^{5-6} years for individual subduction zone volcanoes (White et al., 2006), a single event may transport a volume equivalent to tens of thousands of years of accumulated material. Such collapses are thus major and relatively infrequent events in the history of individual volcanoes.

3. General evidence of magmatic responses to external stress changes

Several external processes have been proposed as causes of significant stress perturbations to stored magma. The best studied of these is ice retreat, particularly following the end of the last glaciation. Evidence from Iceland suggests a substantial increase in volcanism in the late Pleistocene and early Holocene, attributed principally to enhanced melt production (Jull and McKenzie, 1996; Maclennan et al., 2002; Eason et al., 2015).

Glacial unloading is different from sector-collapse induced unloading in two ways. Firstly, deglaciation is a regional-scale effect, and the resultant lithospheric adjustment may drive increased mantle melting (in a rift setting such as Iceland, at least; evidence is more limited in arc settings (cf. Watt et al., 2013; Rawson et al., 2016)), as well as affecting crustally stored magma. In contrast, volcanic edifices represent a local perturbation to the lithostatic stress field (Pinel and Jaupart, 2005). The impact of sector collapse is thus limited to upper crustal magma bodies in arc settings, and is not likely to affect melting processes, with the possible exception of large collapses in ocean-island settings (Presley et al., 1997; Hildenbrand et al., 2004; Manconi et al., 2009) (see Section 8, below). Secondly, the timescale of sector collapse is much more rapid than ice retreat, and the stress change thus exceeds the rate of magmatic processes. This means that sector collapse provides a much clearer natural laboratory than ice retreat to test the impact of surface unloading on stored magma. The effectively instantaneous nature of collapse means that any effects can be placed in a clear stratigraphic context, even if absolute ages are unknown, providing a sharp distinction between pre- and post-unloading conditions.

The rapid nature of sector-collapse induced stress changes is comparable to earthquake induced magmatic stresses (Albino, 2011), but the local static stress change is far larger. A range of evidence supports magma disruption following earthquakes, leading to triggered eruptions within days (Linde and Sacks, 1998; Manga and Brodsky, 2006), to potentially years (Watt et al., 2009b). However, most postulated mechanisms suggest that these effects are due to dynamic stress induced by seismic waves, rather than static stress changes (Hill et al., 2002; Walter and Amelung, 2007).

4. Theoretical effects of sector collapse on magmatic systems

The relationship between magma storage, pressurisation and local crustal stress has been explored through a variety of analytical and numerical approaches (Pinel and Jaupart, 2003, 2005; Gudmundsson, 2006; Manconi et al., 2009; Karlstrom et al., 2015). These models generally assume simplified geometries and physical properties of magma and surrounding rock. Such simplification is justifiable given that constraints on subsurface storage conditions are limited by the spatial resolution and uncertainties of geophysical interpretations (e.g., Foroozan et al., 2010; Paulatto et al., 2012). Petrological studies are increasingly highlighting a complex picture of magma transport, storage and crystallisation (Cashman and Blundy, 2013), suggesting that magma reservoirs may depart significantly from the simplified liquid chamber of theoretical models (Cashman et al., 2017). Nevertheless, it is clear that eruptions are fed by large and relatively homogeneous volumes of eruptible, melt-dominated magma, regardless of how and when these are assembled, and theoretical approaches can thus provide valuable insights into how the volcanic edifice load, or surface loading in general, influences storage conditions and dyke formation.

4.1. Loading, magma storage and dyke formation

An edifice load imposes a departure from a lithostatic stress state in the underlying crust. This effect decreases with depth and becomes negligible at around three times the edifice radius (if the edifice is supported by the strength of the lithosphere; i.e. the edifice radius is small relative to lithospheric elastic thickness) (Pinel and Jaupart, 2005), and is thus most relevant to upper-crustal magma bodies in arc settings. In affecting the local stress field, the edifice load may influence magma chamber growth (Karlstrom et al., 2010; Gudmundsson, 2012), dyke formation (Pinel and Jaupart, 2005; Hurwitz et al., 2009), and dyke propagation (Pinel and Jaupart, 2000; Muller et al., 2001; Kervyn et al., 2009), and focus dyke ascent around a central vent. Dyke formation – the critical precursor to eruption – may be modelled in terms of a rupture criterion for a liquid body in an elastic medium (Fig. 3) (Pinel et al., 2010). Rupture will occur at the maximum pressure above the lithostatic state (i.e. overpressure), P_r, that the host rock can sustain. A linked variable, P_c, describes the pressure at which a dyke will close and an eruption will cease (Pinel et al., 2010). P_r is dependent on reservoir geometry and the stress state of the wall rock. Some models (Pinel et al., 2003; Gudmundsson, 2006) relate P_r to the host-rock tensile strength (cf. Gudmundsson, 2012), but others (Grosfils, 2007; Hurwitz et al., 2009; Gerbault et al., 2012) argue that much higher overpressures can be sustained if gravitational loading is accounted for.

4.2. Edifice growth and eruption rate

Following the analytical approach of Pinel and Jaupart (2003), as an edifice increases in size the load-related tensile stress on a subsurface liquid body increases to a maximum (and P_r and P_c decrease to a minimum; Fig. 3). Beyond this point, increasing edifice growth progressively hinders rupture. A broad range of factors, including reservoir shape, affect the details of this relationship but not the qualitative principles. If an open link to a deeper reservoir is assumed, then the rate of pressurisation of the upper reservoir will be determined by the pressure difference between them (Fig. 3A). When P_r is relatively low, then following an eruption, replenishment of the upper reservoir (i.e. the repressurisation from P_c to P_r; assuming no replenishment during the eruption) will be relatively rapid, and the time to the next eruption correspondingly short (i.e. a high theoretical eruption rate). This therefore predicts that edifice growth is accompanied by an increasing eruption rate, to the point where P_r reaches a minimum, and then a decreasing eruption rate (Pinel et al., 2010) (Fig. 3B). There are large simplifications in this model, including assumptions of constant magma properties and supply rates, and that dykes consistently feed eruptions rather than intrusions, but it nevertheless provides a simple framework to consider the impacts of edifice growth and destruction. It also implies a limit to edifice growth, with the surface load modulating the storage system, which fits with broad observations of a finite lifetime to individual volcanoes and the common occurrence of successively younger edifices adjacent to older, extinct systems (e.g. Singer et al., 1997; Davidson and de Silva, 2000).

4.3. The impact of sector collapse

The simplified theoretical relationship between edifice size, dyke formation and eruption rate allows a range of different scenarios to be postulated following the sudden reduction in edifice load that accompanies edifice collapse (or more accurately, the redistribution of this load across a broader area; Albino et al., 2010; Pinel and Albino, 2013) (Table 1). If sector collapse is triggered by a shallow intrusion or incipient eruption (i.e. a Mount St. Helens type event), then this implies that eruptible magma is present and that the initial P_r criterion has been met. Collapse will always reduce the magma chamber pressure, P_m (Fig. 3), and the nature of the subsequent eruption is dependent on the difference between the resultant P_r and the post-collapse P_m. In some circumstances, a larger eruption may result, but Pinel and Albino (2013) show that for many edifice and chamber geometries, the eruption will be smaller or may stall entirely. For subsequent eruptions, the impact of collapse depends on where the system lies on the P_r curve (Fig. 3) (Pinel and Albino, 2013). Broadly speaking, for edifices at a later stage in the growth cycle outlined above, a load decrease will reduce P_r, favouring conditions for dyke rupture and an increased subsequent eruption rate (Fig. 3). The opposite effect is predicted for smaller edifices. Similar outcomes are predicted if sector collapse is not intrusion-related, but if an eruptible body of magma is present. The newly established stress state may, in some circumstances, result in a P_r that is less than the post-collapse P_m, and in this instance an eruption would be triggered by the collapse. Finally, if no eruptible magma is present, the post-collapse stress state will simply alter the conditions for subsequent dyke formation, if and when an eruptible liquid body forms in the upper crust.

In addition to these effects, and regardless of the change in P_r, the reduction in P_m that accompanies collapse will induce magma ascent from a deeper reservoir, if an open connection exists (Pinel et al., 2013). Sector collapse may therefore initiate the addition of heat or volatiles to the upper reservoir, which may potentially (but not necessarily for larger-volume systems; cf. Ruprecht and Wörner, 2007)) lead to eruption or compositional changes in subsequently erupted magmas.

In general, given that surface loading inhibits the ascent of denser mafic magmas and promotes their stalling in the upper crust (Pinel and Jaupart, 2004), a plausible outcome of collapse is the eruption of more mafic magmas, or of magmas that show a greater influence of a deeper, mafic input. The principle of edifice and chamber co-development acting to influence mafic dyke ascent is supported by observations of outlying vents at Mount Mazama, which become increasingly restricted to locations distant from the central vent prior to the climactic Crater Lake eruption (Karlstrom et al., 2015). In this case, the authors suggest that development of the shallow magma system was driven by increased deep magma influx, but the observation nevertheless supports a relationship between edifice and magma reservoir growth, dyke capture, and a modulation of erupted magma compositions at different stages of volcano development (cf. Schindlbeck et al., 2014).

The theoretical model outlined above (Fig. 3; Table 1) implies that the manifestation of sector collapse on subsequent activity may not follow a common pattern, even before parameters such as magma composition, density and volatile content are accounted for. If these are also considered, it is clear that magmatic responses to sector collapse could be diverse, being dependent on the local load-induced stress state (i.e. the relationship between edifice size and magma reservoir geometry), the nature of the upper crustal magma reservoir at the time of collapse, and the geometry and composition of the crustal plumbing system. Nevertheless, the hypothesis that emerges is that sector collapse results in a sudden shift in eruptive behaviour relative to pre-collapse activity, potentially manifested as a change in eruption frequency, magnitude, composition or style. This would imply that changes in volcanic composition or output do not necessarily reflect changes at the source, but can be modulated from the surface. Past events can be examined in this framework. Conversely, the type of response, if one can be identified, may provide constraints on the nature of the underlying magma reservoir.

5. Volcano growth and eruption-rate measurements

The model outlined in Section 4 implies that changes in eruption rate may be a key manifestation of sector collapse. However, eruption rates can only be accurately defined from recent historical records; even at the best studied volcanoes, reconstructions of prehistoric eruptions are still likely to be highly incomplete (Brown et al., 2014). Beyond historical timescales, the mean volumetric eruptive flux calculated across a defined time period can be used as a proxy for eruption rate. This measurement is reliant on detailed stratigraphic and chronological information and is not a true indicator of eruption rate (since it reflects the magnitude as well as the frequency of eruptions). It also fails to account for intrusive growth of volcanic edifices. Nevertheless, the theoretical relationship in Fig. 3 implies that eruptive flux correlates with eruption rate, and can thus be used to explore variations in eruptive behaviour over prehistoric timescales. Before doing so, it is instructive to assess how well eruptive flux can be determined on timescales of $10^{3\text{-}4}$ years, both in order to interpret observations at volcanoes affected by sector collapse and as a general test of the theoretical relationship between edifice growth and eruption rate.

Measurements of eruptive flux are necessarily time-averaged. On short timescales ($10^{0\text{-}2}$ years), very high values can be maintained (Wadge, 1982), but there is a steady decline in the estimated eruptive flux as the duration of the measurement increases (Fig. 4, inset). Thus, estimates of eruptive flux made over the tens of thousands of years will hide finer-scale variations, and particularly short episodes of elevated output (Hildreth and Lanphere, 1994) such as those that may be expected following sector collapse.

There are relatively few studies that have attempted a detailed quantification of eruptive flux over the lifetime of a volcano. Fig. 4 shows a compilation of thirteen such datasets, all from composite arc volcanoes. Even for these comprehensive field studies, temporal resolution is rarely $<10^4$ years. Erosion and burial, along with dating limitations, mean that age-volume relationships are obscured by multiple uncertainties, and estimates of eruptive flux are likely to be underestimated, with dispersed pyroclastic deposits difficult to account for. Nevertheless, Fig. 4 shows that episodic growth behaviour is a common characteristic of composite arc volcanoes, with relatively short periods characterised by volumetric output rates as much as on order of magnitude greater than relatively quiescent interludes (cf. Davidson and de Silva, 2000). This episodic pattern implies that magma systems remain active across long timescales, even if little extrusion occurs (Hildreth and Lanphere, 1994). Fig. 4 also highlights the decrease in data resolution with time: the highest measured values occur within the past few ten thousand years; before this time, high-flux episodes are generally not resolvable. The average eruptive flux across all these datasets shows that this is not just a smoothing effect, because the long-term mean decreases markedly beyond ~120 ka.

This suggests that erosion, burial and dating limitations all hinder our ability to reconstruct volcanism beyond the most recent episodes of cone-building (cf. Singer et al., 2008). Reconstructions prior to the youngest period of volcanism at any volcano are thus likely to significantly underestimate eruptive flux and are unlikely to resolve variability on timescales below 10^4 years. The temporal resolution at which past activity can be reconstructed therefore remains too coarse to fully test whether edifice growth cycles replicate in detail the shape of the curve predicted in Fig. 3.

Although it is not always clear what divides individual constructional episodes, several studies identify major sector collapse deposits that delineate periods of cone-building (Hall et al., 1999; Thouret et al., 2005; Hora et al., 2007; Hall and Mothes, 2008; Samaniego et al., 2012) and cycles of collapse and regrowth characterise the history of many individual volcanoes (Robin et al., 1990; Zernack et al., 2012; de Silva and Lindsay, 2015). Sector collapse thus appears to be a fundamental process in composite volcano development, and systematic variation in volcanic output may be related both to the maturation of a magma reservoir and the growth of the overlying edifice, even if the details of how post-collapse volcanism differs from pre-collapse activity are not documented. In many cases, collapse scars are buried by rocks erupted during subsequent rapid regrowth (de Silva and Lindsay, 2015), providing general support for enhanced post-collapse activity. However, a more detailed evaluation of this process requires reconstructions that can address whether, by effectively shifting the coupled volcano-magma system to an earlier stage in a theoretical growth cycle, collapse drove a resultant change in eruptive behaviour. To reject the null hypothesis, we must ideally demonstrate that through the rebuilding process, a volcanic system moves back towards its pre-collapse state, thus responding both to the perturbation and to subsequent regrowth.

6. Historical events

Wide recognition of sector-collapse processes came about following the Mount St. Helens eruption of 1980, although earlier eruptions such as those at Bandai (1888) and Bezymianny (1956) had been identified as distinctive in terms of their deposits and horseshoe-shaped scars (cf. Siebert, 1984). The largest historical sector collapse, at Ritter Island (1888), was originally interpreted as a caldera-forming explosive eruption and only later recognised as a sector collapse (Johnson, 1987). These historical events provide only a geologically short window into subsequent activity, potentially insufficient to fully examine the consequences of collapse on the magmatic system, but at least providing information at a high temporal resolution and overcoming the age uncertainties and incompleteness that hinders prehistoric reconstructions.

Historical collapses that meet a >1 km^3 volume criterion are shown in Table 2. Smaller collapses, such as that at Bezymianny (0.5 km^3; Belousov et al., 2007) or the December 2018 collapse of Anak Krakatau, are excluded from the table, but described below in the context of other historical events. Recently revised volumes of the Bandai collapse (Yoshida, 2013) suggest its volume was also <1 km^3, and the Oshima-Oshima (1741) collapse volume is relatively poorly constrained (Table 2). Although these were all major landslides and caused extensive local impacts, they are relatively small in the context of documented prehistoric sector collapses (Fig. 2).

6.1. Eruption-associated collapses

With the exception of Bandai and possibly Ritter, all historical examples of sector collapse were associated with fresh magma ascent. Collapse occurred during an explosive eruption at Oshima-Oshima and Bezymianny, and during a longer-lasting phase of eruptive activity at Anak Krakatau, while the Mount St. Helens collapse was preceded by magma ascent to a shallow level within the edifice. Decompression of the shallow Mount St. Helens intrusion, initiated by landslide movement, resulted in a powerful lateral blast (Glicken, 1996), and a similar effect occurred following conduit depressurisation at Bezymianny (Belousov et al., 2007). At Shiveluch (and also at Harimkotan, 1933 (0.4 km^3; Belousov and Belousova, 1996)) magma was not sufficiently shallow for a directed blast to result (Belousov, 1995), but collapse was preceded by accelerating seismicity and immediately followed by a large explosive eruption, suggesting that an incipient eruption caused these collapses.

It is difficult to assess whether these historical eruptions proceeded differently relative to a hypothetical scenario without collapse (cf. Table 1). However, it is clear that there are no instances among them of a stalled eruption (assuming that the Bandai collapse was not due to magma ascent, which is reasonable given an absence of magma extrusion since 25 ka), which is one of the outcomes of collapse put forward by Pinel and Albino (2013) (Table 1). In all the above cases, the intense explosive eruption that accompanied collapse was followed by an effusive phase (and a phreatomagmatic phase in the case of Anak Krakatau) that partially infilled the collapse scar, which appears to be a common process in eruption-associated sector collapses (Table 2).

At Oshima-Oshima and Bezymianny, collapse followed a long period of quiescence (Satake and Kato, 2001; Belousov et al., 2007; Girina, 2013). However, in both cases it was a renewed eruptive phase that triggered collapse, rather than the reverse. At Oshima-Oshima (and similarly at Harimkotan; Belousov and Belousova, 1996), this eruptive phase declined over the subsequent fifty years (Katsui and Yamamoto, 1981), and there have been no subsequent eruptions. In this case, there is nothing to indicate that the post-collapse state of the system differs significantly from pre-collapse conditions. At Bezymianny, the initial event heralded a period of intense activity that is ongoing today and has largely buried the collapse scar (Girina, 2013), but since this renewed phase of volcanism began prior to the collapse, its origin is likely related to deeper magmatic processes.

6.2. The largest historical collapses: Ritter, Shiveluch and Mount St. Helens

In contrast to Oshima-Oshima and Bezymianny, Shiveluch, Ritter and Mount St. Helens were relatively active volcanoes before collapse and remain so today (Global Volcanism Program, 2013; Day et al., 2015; Watt et al., 2019). At Shiveluch, the 1964 event is just one of multiple Holocene sector collapses (Belousov et al., 1999; Ponomareva et al., 2006) and fits within a long-term pattern of repetitive collapse and regrowth. Similar behaviour is suggested by multiple relatively small (generally ≤1 km^3) collapses at volcanoes such as Stromboli (Tibaldi, 2001), Augustine (Begét and Kienle, 1992) and Harimkotan (Belousov and Belousova, 1996)). Shiveluch is characterised by an unusually high magma flux (Belousov et al., 1999), and the 1964 collapse volume is equivalent to ~10^2 years of magmatic output. In this context, the collapse is relatively minor. It accounted for <1% of the total edifice volume (cf. Grosse et al., 2014), and predominantly involved material extruded since the preceding edifice failure. Regular and relatively small collapses, involving recently erupted material, may be a common outcome of rapid construction at highly active volcanoes. The 1964 event was not unusual in the context of Holocene activity at Shiveluch, and would not, therefore, be expected to mark a major change in behaviour relative to pre-1964 activity. It is also dwarfed by a late-Pleistocene or early-Holocene collapse, which was not accompanied by a major eruption (Ponomareva et al., 2006) but does mark a distinct shift in erupted magma compositions (Belousov et al., 1999; see Section 7).

As suggested at Shiveluch, the significance of sector collapse at a volcano may not be correlated closely with collapse volume, but may be better evaluated in terms of long-term eruptive flux and total edifice volume. In this sense, the Ritter and Mount St. Helens events stand out among historical collapses, in mobilising 10–20% of the edifice (based on edifice volume estimates from Grosse et al. (2014) and Day et al. (2015)). At Ritter, recent observations suggest that the collapse marked a shift in erupted compositions and was also immediately followed by a compositionally anomalous felsic explosive eruption (Watt et al., 2019). This post-collapse eruption was bimodal, containing a mafic phase alongside felsic material that is distinctive in both its glass chemistry and mineral content (containing phenocryst amphibole), and unlike any other known eruption products from Ritter. The eruption is consistent with collapse-driven perturbation of the underlying magma reservoir (see Section 7). Scoriaceous deposits from subsequent eruptions are less compositionally diverse, but comprise a mixture of mafic clasts that are more primitive than pre-collapse material, as well as intermediate compositions, suggesting tapping of discrete crustal magma bodies during post-collapse regrowth of the volcano (Watt et al., 2019). It is unclear if these changes were accompanied by a change in eruption rate; the volcano experienced frequent minor basaltic explosive eruptions before 1888, and similar activity is ongoing within the collapse scar (Day et al., 2015; Watt et al., 2019), implying no major changes in eruption style.

Mount St. Helens is better studied than Ritter, and has been highly active throughout the Holocene. The 1980 collapse followed a pause in activity of ~120 years, and principally involved material erupted over the preceding 2.5 kyr, ranging from basalts to dacites (Glicken, 1996). The collapse and explosive eruption was followed by extrusion of a highly crystalline and gas-poor dacitic lava dome, with no major changes in magma chemistry, suggesting that the event tapped a relatively well-mixed and homogeneous magma body. Broadly similar dacitic magma was erupted in a subsequent dome-building phase from 2004-2008 (Pallister et al., 2008), and both magmas are comparable to those erupted in pre-collapse historical eruptions. The 2004-08 lavas show the least evidence of mixing with a basaltic contaminant for any eruption in the past 500 years (Pallister et al., 2008), and there is no strong evidence to support the input of fresh magma from the lower crust.

Recent eruptions at Mount St. Helens suggest a long-lived dacitic upper-crustal reservoir, with no significant change in post-collapse eruption rates or magma compositions. One notable observation, however, is that the equilibration pressure of the 2004 magma (130 MPa) is significantly lower than that of the magma that initiated the 1980 collapse (220 MPa) (Pallister et al., 2008; Rutherford and Devine, 2008). Pallister et al. (2008) interpret this in a framework of a magma reservoir extending from depths of 5 to 12 km, tapped at different levels by different eruptions. The change in equilibration depth between successive eruptions, in a shallowing pattern, was noted by Gardner et al. (1995) and has characterised two cycles of activity at Mount St. Helens over the past 4000 years. It is, however, unclear why the equilibration depths of magma batches follows a systematic shallowing trend, and Pinel and Jaupart (2003; see also Pinel et al., 2010) offer an alternative explanation. They argue that edifice destruction following large explosive eruptions or sector collapse results in a reduction of the overpressure required to initiate dyke ascent, and that conversely, edifice growth results in higher overpressures. In this model, the equilibration pressures do not reflect depth, but the overpressure sustained in a fixed magma reservoir. Although this is qualitatively consistent with theoretical relationships between edifice growth, chamber pressurisation and replenishment rates (Pinel and Jaupart, 2003), the absolute magnitude of the pressure range during eruptive cycles at Mount St. Helens (up to 180 MPa) is an order of magnitude larger than most estimates of maximum magma reservoir overpressures (Gudmundsson, 2012). Constraints from mineral assemblages and other petrological indicators also support a vertically extensive reservoir, with magma phenocryst mixtures spanning this pressure range (Rutherford and Devine, 2008; Cashman and Blundy, 2013). The post-collapse behaviour of Mount St. Helens doesn't, therefore, fit a simple model of collapse-modulated pressurisation. However, it is possible that the reduction in equilibration pressures is linked to the reduced edifice load, if loading influences the depth range of magma convection, the accumulation depths of mobile magmatic components, or the stalling depth of any mafic, replenishing magma.

7. Magmatic impacts of sector collapse in subduction zone settings

Many of the factors controlling arc magma compositions, including slab input, mantle melting and lower crustal interactions, are not plausibly influenced by sector collapse (see Section 4). Any collapse-associated changes in eruptive behaviour are thus expected to reflect mid- to upper-crustal magma processing, including the timescale of crustal transit, storage and assimilation, the relative proportions and influence of mixing, the ascent and stalling of mafic magmas, and consequent pressure and temperature controls on mineral phase stability. Such processes may be apparent via changes in erupted compositions or eruption rate and style. Evaluating evidence of this for prehistoric collapses requires comparison between pre- and post-collapse magmas at a range of timescales, which is often hindered by limited exposures and poorly resolved age relationships. Although many volcanoes show evidence for rapid post-collapse regrowth and scar burial (e.g., Hora et al., 2007; Samper et al., 2007; de Silva and Lindsay, 2015), this regrowth may prevent sampling of the oldest post-collapse products and inhibit estimates of eruption rates and volumes. For example, the relatively small 1956 collapse scar at Bezymianny has been filled by dome lavas within a few decades (Girina, 2013), representing a rapid extrusion rate that would be unresolvable for more ancient events.

Dating uncertainties also hinder discrimination between rapid (decadal to centennial) and much more gradual shifts in behaviour. There are numerous examples of major collapses where data are too limited to unambiguously correlate specific episodes of volcanism with the timing of collapse (e.g., Galunggung, Indonesia (Bronto, 1989)), or where available data span a restrictive stratigraphic range (e.g., Avachinsky, Kamchatka (Ponomareva et al., 2006)) or are coarsely resolved (e.g., Orizaba, Mexico (Schaaf and Carrasco-Núñez, 2010); St Lucia, Lesser Antilles (Boudon et al., 2013); Baru, Panama (Sherrod et al., 2007)). For the vast majority of identified sector collapses in Fig. 1, stratigraphic resolution and age reconstructions do not enable a robust evaluation of how collapse affected subsequent volcanism. The examples discussed here (summarised in Table 3) are thus limited to a small number of better studied volcanoes. These are also geographically skewed, with detailed studies available from many Andean volcanoes and a notable absence of data from Japan and Indonesia.

7.1. Anomalous post-collapse eruptions

If eruptible magma exists beneath a volcano, regardless of whether an incipient eruption caused the collapse, collapse-driven depressurisation may result in magma ascent or other perturbation of the magma reservoir (cf. Table 1). This is supported by the post-collapse eruption of unusually voluminous or compositionally anomalous lavas at several volcanoes. For example, the 12 km^3 collapse of Chimborazo, Ecuador at 60–65 ka was followed by the eruption of homogeneous andesitic lava flows that extend to distances of 22 km and have a total volume of 1–1.5 km^3 (Samaniego et al., 2012). The Holocene collapse of Antuco, Chile, presents a comparable example, where two unusually thick and far-reaching lava flows directly overlie the debris avalanche deposit (Fig. 5). The Sr-isotope composition of these lavas is more closely aligned with younger post-collapse rocks (unpublished data), but they are less mafic than the basalts that have dominated all subsequent activity at Antuco (Table 3; Martínez et al., 2018). In both cases, the lava-flow volumes are anomalously large in a long-term context of activity at the volcano, and the lava composition is potentially consistent with mixing between a pre-existing magma body and fresh, mafic input, or the disruption of a previously stable (e.g. vertically zoned or compartmentalised) reservoir.

Other examples of anomalously voluminous post-collapse effusive eruptions may include Fuya Fuya (Robin et al., 2009) and Tungurahua I (Hall et al., 1999), both in Ecuador. The latter edifice experienced a large but poorly-exposed collapse at the end of its history, followed by emplacement of voluminous dacite lavas, unusually silicic in the long-term history of the volcano. The andesites erupted during the regrowth of the younger Tungurahua II edifice are geochemically distinct from those of Tungurahua I, indicating establishment of a discrete plumbing system (Hall et al., 1999). Tungurahua II itself collapsed at ~3 ka, and the volcano provides a rare example where collapse-associated shifts in behaviour are replicated over more than one eruptive cycle. The Tungurahua II collapse was followed by voluminous (6-km long) and petrologically distinctive (olivine, two-pyroxene and amphibole-phyric) dacite lava flows, and then a pause in volcanism of ~700 years before rapid regrowth of the andesitic Tungurahua III edifice (Hall et al., 1999). A comparable pattern occurs at San Pedro, Chile, where a mid-Holocene collapse was followed by an unusual composite lava flow with a total volume (0.8 km^3) several times larger than younger summit lavas (Costa and Singer, 2002). The composite flow, representing the earliest post-collapse rocks, differs from both older and younger lavas in containing hornblende phenocrysts. As well as having a bulk composition more felsic than any other Holocene lavas at San Pedro, it contains gabbroic xenoliths and basaltic inclusions that extend to more mafic compositions than other Holocene products (Fig. 5). Costa and Singer (2002) interpret these lavas as representing rapid withdrawal from a zoned upper-crustal reservoir, and infer that their textural complexity developed prior to collapse. However, an alternative explanation is that mixing was induced by unloading, and an absence of intervening material or erosion suggests that the emplacement of these complex lavas occurred shortly after sector collapse.

Post-collapse pyroclastic deposits at Nevado de Colima, Mexico may provide an additional example of decompression-driven disruption of a zoned magma reservoir (Fig. 5). This ~7 km^3 collapse is directly overlain by deposits containing juvenile clasts of mixed composition, including the most mafic material known from the volcano (although more mafic rocks occur at outlying scoria cones) (Robin et al., 1990). At both Colima and San Pedro, compositions that are unknown at the surface in other intervals are observed in the earliest post-collapse rocks, but not in subsequent eruptions. The hornblende-phyric pumice erupted after the 1888 collapse of Ritter Island, which appears to have otherwise erupted relatively homogeneous basalts and basaltic andesites (Watt et al., 2019), provides a comparable example, as do the Secche di Lazzaro deposits at Stromboli (Petrone et al., 2009; see Section 7.2 and Table 3). Collectively, these examples are consistent with anomalous mixing and ascent dynamics following collapse, and highlight that compositions erupted under equilibrium (i.e. without collapse-driven reservoir perturbation) conditions may present an incomplete or biased picture of the compositional range of crustal magmas.

7.2. Post-collapse regrowth through mafic volcanism

A post-collapse shift to more mafic erupted compositions occurs at several volcanoes, maintained over multiple eruptions (Fig. 6). This pattern includes examples with anomalous post-collapse eruptions, such as Antuco, where the voluminous lava flows were followed by more mafic monotonous lavas and scoria deposits that have infilled the collapse scar (representing a higher eruptive flux than pre-collapse activity) and persist to the present day (Martínez et al., 2018). Similarly, at Martinique, the Le Prêcheur collapse is bracketed by two near identical lavas (suggesting post-collapse eruption from an existing magma body), but is followed by a sharp shift to mafic compositions before an eventual return to more evolved magmas (Germa et al., 2011).

Eruptions of relatively mafic magmas may be maintained for several thousand years following collapse, and this is consistent with conditions that favour rapid crustal transit and the ascent of denser magmas to the surface. At Planchón, Chile, pre-collapse basaltic andesites are followed by post-collapse basalts that lack evidence for upper crustal storage (Tormey et al., 1995; Tormey, 2010) and are compositionally similar to the oldest pre-collapse rocks, thus supporting a general cyclical coupling of edifice growth and magma evolution, with increased loading favouring upper crustal stalling of denser, mafic magmas (e.g., Schindlbeck et al., 2014). Alongside more mafic compositions and evidence of reduced storage and assimilation, an elevated eruptive flux is observed in several examples. At Tungurahua, rapid regrowth of the TIII edifice (following the dacite lava eruptions and a 700-year pause in activity) was achieved by volumetric growth rates of ~1.5 km^3/kyr that have persisted since 2.3 ka (Hall et al., 1999). The early stages of this cone rebuilding produced homogeneous basaltic andesites, suggesting relatively rapid crustal transit, but recent magmas are more evolved and may hint at a transition towards more prolonged shallow storage. A broadly similar pattern is suggested by the evolution of Ollagüe, Chile, following a relatively smaller flank collapse (Feeley et al., 1993; Clavero et al., 2004), as well as the examples shown in Fig. 6.

At Parinacota, Chile, the 6 km^3 collapse at 8.8 ka (Jicha et al., 2015) was followed by extremely high eruptive flux of up to 10 km^3/kyr for one to two thousand years, sufficient to entirely bury the collapse scar. Post-collapse rocks are relatively homogeneous and more mafic than pre-collapse lavas (Wörner et al., 1988; Hora et al., 2007, 2009), including the most primitive compositions known at the volcano (Fig. 6). The collapse appears to have occurred within a long-term trend towards more mafic compositions, but regardless of the compositional impact of collapse, the increased post-collapse flux of relatively monotonous magmas represents a sharp change from pre-collapse activity. Evidence for long-term upper-crustal stagnation under pre-collapse conditions contrasts with much more limited evidence of assimilation in younger products (Hora et al., 2009). A spatial change in the post-collapse plumbing system, with a diminished upper crustal reservoir, is also suggested by plagioclase zoning patterns (Ginibre and Wörner, 2007).

Stromboli, Italy, provides a further example of a coupled post-collapse shift in magma chemistry and eruptive behaviour (Francalanci et al., 1989; Bertagnini and Landi, 1996; Tibaldi, 2001, 2004; Petrone et al., 2009; Vezzoli et al., 2014). The 14 ka Upper Vancori collapse (2.2 ± 0.9 km^3) ended a period erupting variable basic and intermediate magmas (Fig. 6), and was followed by more compositionally restricted mafic volcanism (Francalanci et al., 1989; Vezzoli et al., 2014) at a higher volumetric growth rate (Tibaldi, 2004; Vezzoli et al., 2014). These post-collapse magmas are unusually potassic, with relatively monotonous bulk compositions and petrological characteristics. However, their variable Sr-isotope compositions suggests differential assimilation during crustal transit, coincident with the reduction of the upper crustal reservoir (Francalanci et al., 1989; Hornig-Kjarsgaard et al., 1993). The unstable post-collapse cone at Stromboli has failed to achieve the dimensions of the preceding edifice, and has experienced three younger and relatively closely-spaced collapses from ~6 ka (each <50% of the volume of the Upper Vancori collapse; Tibaldi, 2001, 2004), maintaining high growth rates but with a further compositional shift to basaltic shoshonitic magmas following the ~6 ka collapse (Fig. 6), and a predominance of explosive over effusive activity (Francalanci et al., 1989; Hornig-Kjarsgaard et al., 1993)). The Neostromboli eruptive phase, which followed the Upper Vancori collapse and was terminated by a ~1km^3 sector collapse at 6 ka (Tibaldi, 2001), provides additional support to a cyclic model of post-collapse regrowth through mafic volcanism and the re-establishment of a more evolved, upper crustal reservoir (Petrone et al., 2009; Vezzoli et al., 2014). The youngest magmas erupted in this 8 kyr period are also the most evolved Neostromboli rocks (Fig. 6), and derived from fractional crystallisation of the more primitive magmas that fed earlier post-collapse eruptions (Vezzoli et al., 2014). These biotite-shoshonites also fed powerful phreatomagmatic explosive eruptions associated with the 6 ka sector collapse (Petrone et al., 2009), whereas all subsequent volcanism has been more primitive. Thus, since the Neostromboli sector collapse at 6 ka, the upper-crustal reservoir does not appear to have been re-established (Vezzoli et al., 2014). The phreatomagmatic activity that accompanied the Neostromboli collapse (the Secche di Lazzaro eruptions) erupted petrographically heterogeneous products, suggestive of disruption of a complex, stratified shallow plumbing system, and thus consistent with the processes described in Section 7.1 (Petrone et al., 2009). Based on mineral zoning, compositional variability and disequilibrium textures, Petrone et al. (2009) rule out fresh mafic input as a trigger for the Secche di Lazzaro eruptions (and by implication, as a trigger for the Neostromboli collapse); rather, physical and petrological observations are consistent with decompression-driven eruption of shallowly-stored magma as a direct result of the collapse (Bertagnini and Landi, 1996; Petrone et al., 2009). The evolution of Stromboli between the Upper Vancori and Neostromboli collapses thus encapsulates the range of processes described in Sections 7.1 to 7.3, across an 8 kyr period (Fig. 6).

7.3. Re-establishment of upper crustal storage

Longer timescale reconstructions suggest that the mafic activity at volcanoes such as Stromboli, Parinacota and Antuco may represent a temporary cone-rebuilding stage. Edifice regrowth and increased loading may eventually promote upper-crustal storage, manifested as a return to more evolved erupted compositions. The ~32 ka collapse of Pelée, Martinique, initiated a similar pattern to that of the older Le Prêcheur collapse (Germa et al., 2011): pre-collapse andesites were followed by denser basaltic andesites at an elevated eruption rate (inferred from tephra-deposit frequencies and volumetric reconstructions) (Germa et al., 2015). However, within ~10 kyr eruptions returned to predominantly andesitic compositions

(Boudon et al., 2013) (Fig. 6), but enclaves in these young andesites show that deeper mafic magmas were still feeding the newly established upper crustal reservoir.

The evolution of Pelée has a counterpart in the basaltic South Soufrière Hills episode on Montserrat (Cassidy et al., 2015a), which followed the 130 ka D2 collapse and is compositionally anomalous in the long-term history of this andesitic island (Fig. 6). Although the duration of South Soufrière Hills volcanism is difficult to constrain, Cassidy et al. (2015a) suggest that the onset of post-collapse mafic volcanism was rapid (<100 years). Available dates for South Soufrière Hills are also identical within error (Harford et al., 2002), suggesting elevated eruption rates with a maximum duration of a few thousand years. Cassidy et al. (2015a) interpret the basalts to have risen rapidly from mid-crustal depths, suggesting an absent or inactive upper-crustal storage system in the early post-collapse period, in common with the other examples cited above.

Activity at Montserrat returned to andesitic dome-forming eruptions after the South Soufrière Hills episode, erupting rocks similar to pre-collapse lavas but distinctive in containing phenocryst hornblende (this distinction has persisted to the present day) (Harford et al., 2002; Cassidy et al., 2015a). This pattern is replicated at some Andean volcanoes (de Silva et al., 1993), but is the reverse to that observed at Parinacota, where the dominant mineralogy changes from a pre-collapse hornblende andesite to a two-pyroxene assemblage (Wörner et al., 1988). The direction of the change is not necessarily significant, but simply highlights that the re-established crustal plumbing system was distinct in terms of its predominant pressure and temperature conditions from that which existed previously.

7.4. Long-term collapse-induced shifts in storage and plumbing systems

The impacts of large-scale edifice collapse are not always manifested through more mafic erupted compositions of the type described above. This may be because the post-collapse stress regime, although modified from preceding conditions, still promotes upper crustal stalling of denser magmas. In such cases, evidence of enhanced ascent of mafic, lower-crustal magmas may be more subtle. At San Pedro, post-collapse replenishment (following the anomalous lava flows; Fig. 5) led to eruptions of basaltic andesites with similar major-element chemistry to pre-collapse lavas, but with distinct trace-element and isotope signatures (Costa and Singer, 2002). This implies a crustal processing history that is temporally distinct from the pre-collapse magmas. The same conclusion can be drawn at

Chimborazo (Fig. 7; Table 3), Tungurahua (Hall et al., 1999) and elsewhere, where permanent changes in bulk compositional trends support the establishment of a discrete plumbing system, overwriting any influence of older magmatic contributions. There are many other less well studied volcanoes where available data nevertheless hint at post-collapse modification of the plumbing system. Examples include the presence of unusually mafic inclusions in post-collapse lava domes at Tata Sabaya, Bolivia (de Silva et al., 1993), and a change to predominantly effusive activity after the sector collapse of Santa Ana, El Salvador (Siebert et al., 2004).

The very large late-Pleistocene collapse of Shiveluch marks a transition in both chemistry and eruption style (Table 3). Although pre- and post-collapse rocks span a similar range of silica contents, the post-collapse mafic magmas are more primitive (e.g., in terms of Mg#; Table 3) than older equivalents, thus supporting renewed mafic input (Gorbach et al., 2013) (Fig. 7). Compositional trends suggest that pre-collapse magmas predominantly evolved via fractional crystallisation, while post collapse magmas are consistent with mixing between deeper basalts and shallower felsic magmas, interpreted by Gorbach et al. (2013) as indicating a simpler and smaller shallow reservoir in the post-collapse period. Belousov et al. (1999) suggest that these changes had additional consequences for eruption style and edifice stability, producing intermediate magmas with higher viscosity in the post-collapse period, emplaced as lava domes. These built a steep edifice prone to destabilisation upon subsequent intrusion, and susceptible to repeated smaller-scale collapses of the type observed in 1964. In this respect, post-collapse behaviour at Shiveluch mirrors that at Stromboli, over a comparable time period (cf. Tibaldi, 2004).

Observations at several volcanoes suggest that sector collapse focuses shallow dyke propagation towards the collapse scar (Tibaldi et al., 2008), with the vent migrating to the centre of the collapse amphitheatre at volcanoes such as Planchón (Tormey, 2010), Ollagüe and Stromboli (Tibaldi et al., 2008) (comparable processes have also been suggested at ocean-island volcanoes; Maccaferri et al., 2017). Post-collapse rebuilding often buries the scar (e.g., Parinacota), and is generally centred on a similar position to the pre-collapse conduit. Thus, assuming broadly vertical storage geometries, younger magmas appear to pass through preceding storage regions while retaining a discrete chemical signature. The South Soufrière Hills episode at Montserrat is unusual in lying to one side of the collapse scar (cf. Cassidy et al., 2015b), but given observations elsewhere there is no general requirement for post-collapse mafic magmas to bypass upper crustal reservoirs to reach the surface. Indeed, by reaching the surface, the eruption of deeper, mafic magmas implies the absence of a mobile upper crustal reservoir under early post-collapse conditions.

7.5. A coherent model?

The sections above provide several examples where sector collapses mark clear transitions in erupted magma compositions or style of volcanic activity, but these effects are not identical at each volcano. Nevertheless, the observations can fit a single coherent model if inter-volcano differences are attributable to local factors. For example, the volume of a sector collapse, in conjunction with storage depths, reservoir volumes, and the presence of eruptible magma, is likely to determine the observed effect. Notwithstanding these differences, a consistent model emerges from the examples above, summarised in Fig. 8.

7.5.1. Collapse-driven reservoir disruption, or vice versa?

Determining the causal sequence of collapse-associated transitions in volcanic behaviour is challenging. If it is fresh magma input that drives edifice instability, then shifts in magma compositions may simply be temporally associated with sector collapse, but not initiated by the unloading process. However, although it is not possible to definitively exclude this interpretation, large-scale sector collapse provides a plausible mechanism for disruption and reconfiguration of an otherwise stable plumbing system (and one that has developed in equilibrium with the overlying load), whereas no specific mechanism exists for the reverse. The anomalous eruptions described in Section 7.1 followed but did not accompany collapse (i.e. they are not present as syn-collapse pyroclastic deposits or juvenile debris-avalanche blocks), suggesting that magma ascent did not precede or trigger collapse in these instances. Petrone et al. (2009) present a rare example where detailed mineralogical analyses are used to specifically exclude the possibility of fresh magmatic input prior to the Neostromboli collapse, implying that the intense phreatomagmatic eruptions associated with the collapse directly reflect decompression-driven disruption of the shallow system, and supporting the above interpretation. The replication of compositional anomalies in several examples, contemporaneous with collapse but absent in both older and younger rocks, lends further support for a discrete external process (i.e. sector collapse) driving this atypical behaviour, and one that falls outside the prevailing factors that govern magma storage and eruption at other times in a volcano's history. This argument is also supported by the sharpness of the compositional shifts between pre- and post-collapse magmas (Figs. 6 and 7), which imply the development of a structurally distinct plumbing system during post-collapse regrowth. The interpretation presented here suggests that erupted magma compositions spanning sector collapses are governed by upper crustal processes that reflect the interaction between edifice loads and the stability and growth of shallow magma reservoirs. They do not require (but nor do they exclude) any variation in the flux or ascent of deeper, primitive magmas, but the capacity of such magmas to reach the surface, rather than being captured within shallow reservoirs, may vary as a result of the prevailing upper crustal conditions.

7.5.2. Persistent impacts on plumbing systems and cyclic development

Although the precise age and duration of the compositionally anomalous eruptions described above are not generally constrained, their stratigraphic position directly overlying debris avalanche deposits or pre-collapse rocks (e.g., Ritter, Stromboli, Antuco; Table 3), generally as a single eruptive unit, suggests that they represent short-lived events that potentially occurred immediately after collapse. In contrast, subsequent periods of more persistent mafic volcanism may span time intervals of several thousand years (Fig. 6). This suggests that the compositionally anomalous eruptions mark the death of a plumbing system that is out of equilibrium with the collapse-modified surface load. That anomalous eruptions are not observed after all large sector collapses may simply reflect that eruptible magma wasn't present at the time of collapse (Fig. 8), or that post-collapse stress conditions were not favourable to magma ascent (Table 1) – one of the outcomes predicted by Pinel and Albino (2013). The former interpretation is more consistent with observations: if the upper crustal reservoir is retained after collapse, but magma ascent is simply temporarily hindered, then this can't explain long-term changes in erupted compositions. The fact that sharp compositional changes are observed in multiple examples, coeval with collapse, implies more fundamental impacts on plumbing systems, leading to a post-collapse magmatic regime that is discrete from the preceding one.

The eruption sequences at San Pedro, Tungurahua, Antuco, Stromboli and elsewhere can thus be interpreted in a framework of a pre-existing mobile reservoir, where unloading drives mixing of a previously stagnant magma body. In this interpretation, the earliest post-collapse magmas would not have erupted without sector collapse. It is notable that several of these anomalous eruptions were effusive (Hall et al., 1999; Costa and Singer, 2002; Martínez et al., 2018), and not necessarily initiated by high overpressures or the ascent of volatile-rich magmas from the lower crust, but simply by upper crustal decompression (cf. Petrone et al., 2009).

Other examples, such as Soufrière Hills, Pelée and Tungurahua, support a coupling between edifice growth and magma storage, whereby post-collapse eruptions of deeper, mafic compositions are followed by a return to more evolved compositions (Hall et al., 1999; Boudon et al., 2013; Cassidy et al., 2015a) upon partial edifice regrowth and the re-establishment of upper-crustal stalling of denser, mafic magmas. Longer timescale observations thus support a broad cyclicity of mafic to evolved volcanism, delineated by collapses, which are followed by sharp shifts to more mafic erupted compositions. This provides strong evidence that collapse is followed by the establishment of a storage and plumbing system distinct from the preceding one and, by implication, supports an inherent coupling between surface loading and the factors controlling magma storage and ascent.

The observation of sharp and wholesale shifts in magma composition calls into question models of magma storage that propose long-lived and large-volume liquid bodies, because it is difficult to conceive how such bodies could be bypassed or sufficiently diluted by younger magmas to erase preceding compositional signatures. Rather, reservoirs dominated by crystal mushes, susceptible to becoming immobile over short timescales, are more consistent with observations that require rapid adjustment of upper crustal plumbing systems to enable changes in dominant storage depths and the transit of magmas with persistently different assimilation and crystallisation histories.

7.5.3. Counter-examples and historical collapses

Many arc volcanoes affected by sector collapse have only limited age and compositional data, and even examples with better stratigraphic constraints, such as those in Fig. 6, may suffer from data gaps of many thousands of years or unresolvable age relationships. An absence of mafic post-collapse magmas (e.g., de Silva et al., 1993), or even an apparent shift to more felsic post-collapse compositions (e.g. Boudon et al., 2013), may thus be attributable to sparse stratigraphic reconstructions (cf. collapses on Martinique and St Lucia, much older than those outlined above, where the time gap between collapse and the next dated eruption is poorly resolved; Boudon et al., 2013), and may also be affected by burial of the earliest post-collapse magmas.

At all arc volcanoes with high-resolution stratigraphic reconstructions spanning large-volume (several cubic kilometres; Table 3) sector collapses, the observations are consistent with the processes outlined in Fig. 8. However, with the exception of Ritter Island in 1888 (Watt et al., 2019), historical sector collapses show no such dramatic impacts on the underlying magma system. This may simply reflect the small magnitude of historical events (Table 2) relative to those in Table 3. The 1964 collapse at Shiveluch, for example, involved a fraction of the material mobilised in its late-Pleistocene collapse. If collapse-induced stress changes are comparable to those experienced by crustal magma reservoirs during normal cycles of pressurisation and eruption, then the plumbing system may withstand the impacts of collapse without major modification. Similar behaviour is observed in general eruptive activity: small eruptions fit within coherent trends of composition and style, while major eruptions, involving several cubic kilometres of magma, may mark sharp transitions in behaviour (e.g. Schindlbeck et al., 2014; Gavrilenko et al., 2016). What is notable about sector collapse is that the magma plumbing system may be modified without evacuation of the upper crustal reservoir. This implies that material within the pre-collapse reservoir remains in the crust, but a new plumbing system, giving rise to distinct compositions and evolutionary trends, can overprint the former regime.

Taranaki, New Zealand, provides an example of a volcano that may not fit into the scheme outlined above. Although Taranaki's rocks display a gradual evolution to more evolved and more potassic compositions over its 130 kyr lifetime (Zernack et al., 2012), available data show no apparent sharp changes in magma composition following collapse (post-collapse stratigraphic constraints are, however, absent beyond the Holocene, due to burial during younger regrowth cycles). The volcano is remarkable for the number of identified collapses, and although their precise volume is difficult to constrain (Zernack et al., 2009, 2011), several appear to be comparable in scale to the events in Table 3 (Zernack et al., 2012). The collapse frequency is not as high as that at Augustine (Béget and Kienle, 1992) and Shiveluch (Belousov et al., 1999; Ponomareva et al., 2006), but the larger average collapse volume suggests that Taranaki, like these volcanoes, is characterised by a notably high magma flux and edifice growth rate. This elevated flux may limit the coupling between surface loads and the upper crustal plumbing system, if edifice growth outpaces the crustal response. This is suggested by the relatively constant long-term effusive flux at Taranaki (Zernack et al., 2012), which contrasts with the more pulsatory eruptive flux observed at many volcanoes. (Fig. 4).

8. Collapses at intraplate ocean islands

Intraplate ocean islands represent a second volcano-tectonic setting where several comprehensive studies have identified large-scale flank collapses (e.g., Moore et al., 1989; Masson et al., 2002, 2008), and where the question of how collapse affects magma generation and storage has been addressed by different authors (cf. Longpré et al., 2009; Manconi et al., 2009; Boulesteix et al., 2012; Hunt et al., 2018). Despite the common physical process of gravitational unloading, the magmatic impacts of ocean-island collapses should be evaluated separately to subduction zone volcanoes for a number of reasons. First, ocean islands are dominated by mafic volcanism and do not typically develop long-lived upper-crustal plumbing systems characterised by intermediate to evolved magmas (even if shallow mafic reservoirs develop; cf. Clague, 1987; Frey et al., 1991; Amelung and Day, 2002; Galipp et al., 2006; Hildner et al., 2012). With limited shallow magma storage and without evolved compositions, the influence of loading on magma plumbing systems may be more poorly developed than in arc settings. This is not true of all ocean islands, however, with locations such as Tenerife, Canary Islands, producing large explosive eruptions of felsic magma (e.g., Bryan et al., 1998). Second, the dimensions of ocean islands (Figure 1) are in some cases comparable to the elastic thickness of the underlying (oceanic) lithosphere, and the dimensions of collapse-driven mass redistribution may even be significant in this context. Unlike arc settings, it cannot be assumed that the island mass is supported by the strength of the lithosphere, and there may be an isostatic response to landslide mass redistribution (cf. Smith and Wessel, 2000), and potentially an influence on melt production through mantle decompression (e.g., Presley et al., 1997). Finally, there are variable spatial relationships between flank collapses on ocean islands and the underlying plumbing system. The aspect ratio of collapses is generally lower (Figure 1), despite very large collapse volumes, and collapses may not necessarily overlie the central plumbing system due to the rift-zone structure that characterises many ocean islands (cf. the Orotava and Güímar collapses on Tenerife (Fig. 9), which lie on a rift zone outside the central Cañadas caldera structure; Martí et al., 1997; Carracedo et al., 2011).

8.1. Evidence of plumbing system modifications

Pressure constraints at several ocean islands suggest pre-eruptive magma storage at upper mantle depths, but observations imply that such deep plumbing systems can nevertheless be directly influenced by sector collapse (Table 4). At Fogo, Cape Verde Islands, magmas erupted after the Monte Amarelo collapse (123-62 ka) equilibrated at greater depths (~25 km) than pre-collapse magmas (~18 km), which showed a long-term shallowing trend prior to collapse (although the absolute timescale of this is not well constrained; Hildner et al., 2012) (Fig. 10). Subsequent post-collapse regrowth involved magmas with a shallower and broader range of storage depths, suggesting development of an increasingly complex crustal plumbing system. A broadly similar pattern, spanning comparable depth ranges, has been identified at La Palma, Canary Islands, where the Bejenado volcano grew rapidly after the Cumbre Nueva collapse (560 ka; Guillou et al., 1998; Galipp et al., 2006) (Fig. 10). Younger Bejenado magmas show evidence of increased fractional crystallisation and possibly decreasing magma supply rates as the edifice developed, and the range of storage depths suggests entirely distinct pre- and post-collapse plumbing systems (Galipp et al., 2006).

A detailed evaluation of shield-basalt sequences at the Teno massif, Tenerife, highlights further distinctive shifts in volcanism (Longpré et al., 2009) associated with two >20-25 km^3 landslides. These landslides interrupt and sharply reverse long-term trends towards more silicic and less magnesian lavas, and appear to have disrupted the pre-existing plumbing system. They resulted in explosive eruptions from minor shallow reservoirs (unusual in the long-term effusion-dominated context of the shield) and enabled the ascent and eruption of deep, dense, crystal-rich mafic magmas in the early post-collapse period. Similar patterns follow the El Golfo collapse on El Hierro, Canary Islands (Manconi et al., 2009), where the pre-collapse stratigraphy includes evolved compositions (trachytes). Such rocks are absent in the post-collapse stratigraphy, which is dominated by mafic, crystal-rich lavas. Numerical models (Manconi et al., 2009) suggest that pressure changes in the deep plumbing system, on the order of 1 MPa, are sufficient to disrupt stored magma, drive volumetric expansion and potentially initiate fracturing and dyke ascent.

Volcan Ecuador, in the Galapagos, provides a further example where sector collapse is associated with a shift in the locus of volcanism following disruption of the shallow plumbing system (comparable to changes in vent distribution following the SW landslides on Mauna Loa, Hawaii (Lipman et al., 1990)), and where post-collapse magmas have elevated MgO contents, suggesting favourable ascent of mafic melts (Geist et al., 2002). Shifts in vent location, associated with modified magma ascent paths under post-collapse conditions, have been observed in many ocean island (and some arc) settings (cf. Maccaferri et al., 2017) and may play a role in the development of discrete post-collapse plumbing systems. A direct relationship between rift-zone configuration and flank stability has been proposed at La Palma (Day et al., 1999a), and on Tenerife it has been proposed that rift-zone reorganisation is a direct consequence of large-scale flank collapses (Walter et al., 2005), which may also promote more centralised and evolved subsequent volcanism (Carracedo et al., 2011). Maccaferri et al. (2017) propose that post-collapse stress redistribution, focusing dyke ascent towards the collapse scar, can potentially act as a feedback mechanism promoting edifice regrowth and subsequent collapses in the same area. Such a mechanism may be particularly influential following very large volume collapses in a neutral tectonic environment, as characterised by many ocean-island volcanoes. As suggested by the evolution of the NE rift zone on Tenerife, focusing of volcanism within collapse scars can ultimately promote shallow magma storage, differentiation, and the eruption of more evolved magma compositions (Carracedo et al., 2011). Thus, the structural as well as the magmatic evolution of islands such as Fogo (Day et al., 1999b; Maccaferri et al., 2017) and Tenerife (Carracedo et al., 2011) may directly reflect the past history of sector collapse.

The above examples indicate that although storage conditions and depth ranges may differ from arc settings, the cyclic pattern of plumbing system modification at ocean-island volcanoes, characterised by the transit of deeper magmas via simpler ascent routes in the post-collapse period, with concomitant shifts in chemistry, petrography, and possibly eruption style and vent position (Table 4), is comparable to the cone-rebuilding phase in Fig. 8. This implies that collapse-initiated reorganisation of magmatic plumbing systems is a general process.

8.2. Impacts on shallow magma reservoirs

Tenerife is unusual among ocean islands in having a central, large-volume shallow reservoir, dominated by evolved compositions (Carracedo et al., 2007) (Fig. 9). Indeed, large-scale sector collapses have been cited as a possible reason for the absence of shallow reservoirs on some other ocean islands (Amelung and Day, 2002; Geist et al., 2002). The cyclic Bandas del Sur ignimbrite deposits on Tenerife (Bryan et al., 1998, 2002; Brown et al., 2003; Edgar et al., 2007) show that evolved magmas have been erupted for prolonged periods of the island's recent history, and the impact of the Icod collapse (~175 ka) on the shallow reservoir (Carracedo et al., 2007; Boulesteix et al., 2012) provides further evidence that large ocean island landslides impact magma plumbing systems in an essentially identical way to that observed in arcs.

The Icod landslide deposit is associated with phonolitic pumiceous deposits, but the base of the collapse scar is infilled by mafic lavas, which were erupted at elevated rates over a 10 kyr period (Boulesteix et al., 2012). Regrowth is interpreted to have led to stalling of mafic magmas, accompanied by eruption of increasingly evolved compositions at decreasing rates. This ultimately led to the growth of the phonolitic Teide volcano, fed from an established upper crustal reservoir (Fig. 9). This sequence replicates very closely the model put forward in arc settings, and shows the same transitions in magma composition and storage, on a broadly similar timescale, observed at Montserrat, Martinique and the other examples cited above (Fig. 8).

It is clear that an evolved upper-crustal reservoir existed at the time of the Icod collapse. Phonolitic pumice deposits consistent in age and composition with the Abrigo ignimbrite (Fig. 9) are both cut by the landslide and appear in collapse-associated breccias (Boulesteix et al., 2012), as well as appearing in the upper units of the Icod turbidite (Hunt et al., 2018) and tsunami deposits (Paris et al., 2017). This suggests that a large explosive eruption occurred in the latter stages of collapse, but that similar magma had also fed previous eruptions. Whether an incipient explosive eruption (i.e. shallow magma ascent) led to collapse, or if the accompanying eruption was truly collapse-triggered, cannot be deduced. In any case, the next erupted lavas were mafic and no phonolitic deposits appear in the younger stratigraphy for tens of thousands of years, replicating the patterns of mafic renewal observed at arc volcanoes following termination of the upper crustal storage system.

Hunt et al. (2018) suggest that the pattern of contemporaneous pumice clasts occurring in the upper units of collapse-derived turbidites is replicated by the Orotava collapse (~535 ka) on Tenerife (possibly linked to the Granadilla eruption at 560-600 ka). A collapse-triggered eruption seems less likely in this case, given the location of the Orotava landslide outside the central caldera structure on Tenerife (Fig. 9), but it is plausible that pre-eruptive unrest led to the collapse.

8.3. A direct influence on melting?

Chemical evidence in support of a direct influence of collapse on mantle melt fraction is provided by Hildenbrand et al. (2004) from Tahiti, where the 0.87 Ma collapse is followed by a 90 kyr period of elevated eruptive flux, interpreted as the result of increased melt production. Post-collapse trace-element and isotopic signatures are consistent with higher degrees of mantle melting (Fig. 10). A gradual reversal of this chemical signature, concomitant with a reduced eruptive flux, further supports a relationship between surface loading and mantle melt fraction, although parts of this longer-term trend may be associated with plate movement away from the plume head.

A comparable pattern has been suggested for the evolution of Waianae volcano, Oahu, Hawaii, where an onshore landslide scar marks the interval between the Palehua and Kolekole members (Presley et al., 1997). Gradual evolution of the pre-collapse Palehua lavas is consistent with a decrease in partial melting of 1-2 % through time, but the post-collapse Kolekole lavas mark a sharp reversal of this pattern, consistent with a 1-2 % increase in partial melting (Presley et al., 1997). Kolekole lavas are less differentiated and equilibrated at greater depths than the preceding Palehua magmas. This pattern replicates observations at Fogo and La Palma, while also suggesting, like Tahiti, a relationship between growth, collapse and mantle melt fraction. Presley et al. (1997) suggest that the volume of the Waianae slump is more than sufficient to explain the increase in partial melting implied by post-collapse lava compositions. However, their assumptions may substantially overestimate the impacts of decompression at melt-source depths (>80 km; Watson and McKenzie, 1991) (cf. Manconi et al., 2009; Longpré et al., 2009). Changes in melt fraction and magma compositions, comparable to those at Waianae, have not been documented for other Hawaiian landslides (although renewed episodes of post-collapse volcanism have been noted following some of these (cf. Presley et al., 1997)), and the calculations of Manconi et al. (2009) suggest that, even for these very large collapses, there would not be a significant influence of landslide mass redistribution on melt production.

9. Summary and conclusions

Despite severe limitations in stratigraphic reconstructions, disparate data types, and potential magmatic responses that span a range of timescales, a common pattern emerges from this investigation of the impact of large-scale sector collapses on volcano-magmatic systems. Observations are consistent with an intrinsic relationship between surface loading and the development of mid- to upper-crustal magma reservoirs, indicating that changes to surface loading can modulate magma ascent and storage, and are thereby manifested by shifts in erupted compositions, eruption rate and style. Discrete, rather than gradual, shifts in eruptive behaviour, replicated at several volcanoes and concomitant with collapse, implies that wholesale and fundamental changes to the magma plumbing system can be driven by sector-collapse. This pattern is apparent in examples across both arc and intraplate settings. It is thus reasonable to infer that the impact of large-volume sector collapse on underlying magma reservoirs is independent of tectonic setting, even though data don't currently exist to test this at rift or continental intraplate volcanoes.

Large sector collapses may be followed by compositionally anomalous and notably large-volume eruptions, which are often effusive. This short-timescale response is, however, dependent on the presence of eruptible (i.e. with sufficient liquid proportions) magma in the crustal reservoir, and is therefore not observed in all cases. The anomalous composition of such eruptions implies disruption of an otherwise stable reservoir, and suggests that compositions tapped from this reservoir during typical (i.e. unperturbed by collapse) periods of volcanism are not fully representative of crustal magma compositions. These anomalous events represent truly triggered eruptions (in contrast to eruption-triggered collapses, of the Mount St. Helens type), and are not dependent on magma ascent driving the initial collapse. They thus imply that surface mass redistribution alone has the potential to disrupt stored magma bodies and initiate magma ascent. Although theoretical relationships suggest that collapse is not necessarily expected to favour this process, such models are based on simplified physical and geometrical assumptions that may not well represent a vertically extensive, crystal-rich plumbing system. Thus, although the absence of triggered eruptions in some cases could be consistent with post-collapse conditions that hinder dyke formation, they could equally be explained by an absence of eruptible magma. The latter explanation is more consistent with subsequent compositional changes in erupted magmas at volcanoes affected by large-scale sector collapse.

There are multiple examples of sector collapses followed by a temporary (lasting 10^{3-4} years) shift to eruption of more mafic compositions, often at elevated eruption rates. Such behaviour indicates that deeper, denser magmas can ascend to the surface without capture by a more evolved upper-crustal reservoir. This implies both that surface loading may modulate mafic magma stalling, and that solidification of the existing upper-crustal reservoir, to the extent that mafic magmas can ascend to the surface, is a common result of large-scale sector collapse. On longer timescales, upper-crustal storage is re-established following edifice regrowth, with a transition towards eruption of more evolved compositions at eruption rates comparable to pre-collapse activity. Volcano growth and collapse, with a co-developing crustal plumbing system, can therefore be defined within a broadly cyclic pattern of behaviour, on timescales of 10^{4-5} years in arc settings. This supports theoretical relationships that have previously been proposed, although stratigraphic reconstructions remain too coarse and incomplete to provide a quantitative analysis of this cyclicity. Broadly similar behaviour is observed in intraplate ocean-island settings, but the absence of an evolved shallow reservoir in many instances results in less clear compositional shifts than those outlined above. Nevertheless, post-collapse changes in behaviour at ocean islands can be explained via plumbing system disruption, and enhanced melt production is not a necessary part of the general relationship between collapse and subsequent eruptive behaviour.

The relationships described above are evident in multiple examples of large-volume sector collapses, generally with volumes exceeding 5 km^3. These events are significantly larger than historical sector collapses, with the exception of Ritter Island. The absence of such clear post-collapse responses following historical examples may thus be attributed to the smaller scale of these events, both in absolute terms, and potentially as a proportion of the reservoir and edifice volumes. The load redistribution associated with smaller collapses may be comparable to volumetric and pressure changes during typical eruptive behaviour, and insufficient to drive major changes to the plumbing system (the impacts may potentially be accommodated by decompression within the reservoir (e.g., Voight et al., 2010), and a steady-state is thus maintained). In contrast, the largest sector collapses, much less frequent in the history of individual volcanoes, result in disequilibrium between the crustal reservoir and surface load, marking major shifts in the long-term development of a volcano-magmatic system. The magnitude of collapse is thus significant in terms of its magmatic impact, although investigating the detail of this relationship is again constrained by limitations in reconstructing collapse volumes and magma fluxes.

It is notable that surface mass redistribution alone can drive reorganisation of the upper crustal plumbing system, without large scale magmatic eruption. In such cases, magma within the pre-collapse reservoir remains in-situ, yet post-collapse mafic activity indicates that subsequent eruptions can be fed by magma ascending through this reservoir. Furthermore, isotopic, mineralogical and trace-element characteristics of post-collapse evolved magmas imply that post-collapse upper-crustal reservoirs, although occupying a similar depth range, represent a discrete plumbing system, not directly related to the pre-collapse storage system. Taken together, these observations are consistent with a vertically extensive and crystal-dominated crustal plumbing system beneath volcanoes, since it is difficult to envisage a large-volume, liquid dominated system resulting in such sharp changes in behaviour.

The patterns discussed here are based on a relatively small number of examples, representing all available cases where chemical, chronological, stratigraphic and volumetric data are sufficient to assess pre- and post-collapse patterns in volcanism. Even in these instances, the impact of collapse can only be analysed at a low resolution. Further testing of the processes outlined here, and the theoretical relationships that imply episodic development of volcanic systems and modulation of magma storage by surface loading, is reliant on a greater number of more detailed investigations of individual volcanoes affected by sector collapse, combining compositional and stratigraphic information on timescales spanning tens of thousands of years. The value of such studies lies not simply in improving the understanding of individual systems, but in providing essential insights into the fundamental controls on magma storage, eruptive behaviour, and the nature of magma reservoirs.

Acknowledgements
This work was supported by Natural Environment Research Council (NERC) grant NE/I02044X/1 & 2. Discussions with V. Pinel provided valuable insights into modelling the impacts of sector collapse on magma bodies. I thank T. Horscroft and J. Martí for the invitation to submit this manuscript, and an anonymous reviewer for detailed and constructive comments that improved the manuscript.

References

Ablay, G.J., Carroll, M.R., Palmer, M.R., Martí, J., Sparks, R.S.J., 1998. Basanite–phonolite lineages of the Teide–Pico Viejo volcanic complex, Tenerife, Canary Islands. Journal of Petrology, 39: 905-936.

Ablay, G.J., Hürlimann, M., 2000. Evolution of the north flank of Tenerife by recurrent giant landslides. Journal of Volcanology and Geothermal Research, 103: 135-159.

Albino, F., 2011. Modélisation des interactions magma-encaissant: applications aux zones de stockage et aux conduits de volcans andésitiques, PhD thesis, Université de Grenoble, France.

Amelung, F., Day, S., 2002. InSAR observations of the 1995 Fogo, Cape Verde, eruption: Implications for the effects of collapse events upon island volcanoes. Geophysical Research Letters, 29: 1606.

Bacon, C.R., Lanphere, M.A., 2006. Eruptive history and geochronology of Mount Mazama and the Crater Lake region, Oregon. Geological Society of America Bulletin, 118: 1331-1359.

Begét, J.E., Kienle, J., 1992. Cyclic formation of debris avalanches at Mount St Augustine volcano. Nature, 356: 701-704.

Belousov, A., Belousova, M., 1996. Large scale landslides on active volcanoes in the 20th century - Examples from the Kurile-Kamchatka region (Russia). In: K. Senneset (Editor), Landslides. Balkerna, Rotterdam, pp. 953-957.

Belousov, A., Belousova, M., Chen, C.H., Zellmer, G.F., 2010. Deposits, character and timing of recent eruptions and gravitational collapses in Tatun Volcanic Group, Northern Taiwan: Hazard-related issues. Journal of Volcanology and Geothermal Research, 191: 205-221.

Belousov, A., Belousova, M., Voight, B., 1999. Multiple edifice failures, debris avalanches and associated eruptions in the Holocene history of Shiveluch volcano, Kamchatka, Russia. Bulletin of Volcanology, 61: 324-342.

Belousov, A., Voight, B., Belousova, M., 2007. Directed blasts and blast-generated pyroclastic density currents: a comparison of the Bezymianny 1956, Mount St Helens 1980, and Soufriére Hills, Montserrat 1997 eruptions and deposits. Bulletin of Volcanology, 69: 701-740.

Belousov, A.B., 1995. The Shiveluch volcanic eruption of 12 November 1964 - explosive eruption provoked by failure of the edifice. Journal of Volcanology and Geothermal Research, 66: 357-365.

Bertagnini, A., Landi, P., 1996. The Secche di Lazzaro pyroclastics of Stromboli volcano: a phreatomagmatic eruption related to the Sciara del Fuoco sector collapse. Bulletin of Volcanology 58: 239-245.

Boudon, G., Villemant, B., Le Friant, A., Paterne, M., Cortijo, E., 2013. Role of large flank-collapse events on magma evolution of volcanoes. Insights from the Lesser Antilles Arc. Journal of Volcanology and Geothermal Research, 263: 224-237.

Boulesteix, T., Hildenbrand, A., Gillot, P.Y., Soler, V., 2012. Eruptive response of oceanic islands to giant landslides: New insights from the geomorphologic evolution of the Teide-Pico Viejo volcanic complex (Tenerife, Canary). Geomorphology, 138: 61-73.

Bronto, S., 1989. Volcanic geology of Galunggung, West Java, Indonesia. PhD Thesis, University of Canterbury, New Zealand, 490 pp.

Brown, R.J., Barry, T.L., Branney, M.J., Pringle, M.S., Bryan, S.E., 2003. The Quaternary pyroclastic succession of southeast Tenerife, Canary Islands: explosive eruptions, related caldera subsidence, and sector collapse. Geological Magazine, 140: 265-288.

Brown, S.K., Crosweller, H.S., Sparks, R.S.J., Cottrell, E., Deligne, N.I., Guerrero, N.O., Hobbs, L., Kiyosugi, K., Loughlin, S.C., Siebert, L., Takarada, S., 2014. Characterisation of the Quaternary eruption record: analysis of the Large Magnitude Explosive Volcanic Eruptions (LaMEVE) database. Journal of Applied Volcanology 3: 5.

Bryan, S.E., Martí, J., Cas, R.A.F., 1998. Stratigraphy of the Bandas del Sur Formation: an extracaldera record of Quaternary phonolitic explosive eruptions from the Las Cañadas edifice, Tenerife (Canary Islands). Geological Magazine, 135: 605-636.

Bryan, S.E., Martí, J., Leosson, M., 2002. Petrology and geochemistry of the Bandas del Sur Formation, Las Cañadas edifice, Tenerife (Canary Islands). Journal of Petrology 43, 1815-1856.

Capra, L., Macías, J.L., 2002. The cohesive Naranjo debris-flow deposit (10 km3): A dam breakout flow derived from the Pleistocene debris-avalanche deposit of Nevado de Colima Volcano (Mexico). Journal of Volcanology and Geothermal Research, 117: 213-235.

Carracedo, J.C., 1994. The Canary Islands: An example of structural control on the growth of large oceanic-island volcanoes. Journal of Volcanology and Geothermal Research 60: 225-241.

Carracedo, J.C., Badiola, E.R., Guillou, H., Paterne, M., Scaillet, S., Pérez Torrado, F.J., Paris, R., Fra-Paleo, U., Hansen, A., 2007. Eruptive and structural history of Teide Volcano and rift zones of Tenerife, Canary Islands. Geological Society of America Bulletin, 119: 1027-1051.

Carracedo, J.C., Guillou, H., Nomade, S., Rodríguez-Badiola, E., Pérez-Torrado, F.J., Rodríguez-González, A., Paris, R., Troll, V.R., Wiesmaier, S., Delcamp, A., Fernández-Turiel, J.L., 2011. Evolution of ocean-island rifts: The northeast rift zone of Tenerife, Canary Islands. Geological Society of America Bulletin, 123: 562-584.

Carrasco-Núñez, G., Díaz-Castellón, R., Siebert, L., Hubbard, B., Sheridan, M.F., Rodríguez, S.R., 2006. Multiple edifice-collapse events in the Eastern Mexican Volcanic Belt: The role of sloping substrate and implications for hazard assessment. Journal of Volcanology and Geothermal Research, 158: 151-176.

Cashman, K., Blundy, J., 2013. Petrological cannibalism: the chemical and textural consequences of incremental magma body growth. Contributions to Mineralogy and Petrology, 166: 703-729.

Cashman, K.V., Sparks, R.S.J., Blundy, J.D., 2017. Vertically extensive and unstable magmatic systems: A unified view of igneous processes. Science, 355: eaag3055.

Cassidy, M., Edmonds, M., Watt, S.F.L., Palmer, M.R., Gernon, T.M., 2015. Origin of basalts by hybridization in andesite-dominated arcs. Journal of Petrology, 56: 325-346.

Cassidy, M., Taylor, R.N., Palmer, M.R., Cooper, R.J., Stenlake, C., Trofimovs, J., 2012. Tracking the magmatic evolution of island arc volcanism: Insights from a high-precision Pb isotope record of Montserrat, Lesser Antilles. Geochemistry, Geophysics, Geosystems, 13: Q05003.

Cassidy, M., Watt, S.F.L., Talling, P.J., Palmer, M.R., Edmonds, M., Jutzeler, M., Wall-Palmer, D., Manga, M., Coussens, M., Gernon, T.M., 2015. Rapid onset of mafic magmatism facilitated by volcanic edifice collapse. Geophysical Research Letters, 42: 4778-4785.

Clague, D.A., 1987. Hawaiian xenolith populations, magma supply rates, and development of magma chambers. Bulletin of Volcanology, 49: 577-587.

Clavero, J., Polanco, E., Godoy, E., Aguilar, G., Sparks, R.S.J., Van Wyk de Vries, B., de Arce, C.P., Matthews, S., 2004. Substrata influence in the transport and emplacement mechanism of the Ollague debris avalanche (Northern Chile). Acta Vulcanologica, 16: 59-76.

Coombs, M.L., White, S.M., Scholl, D.W., 2007. Massive edifice failure at Aleutian arc volcanoes. Earth and Planetary Science Letters, 256: 403-418.

Costa, F., Singer, B., 2002. Evolution of Holocene dacite and compositionally zoned magma, Volcán San Pedro, southern volcanic zone, Chile. Journal of Petrology, 43: 1571-1593.

Coussens, M., Wall-Palmer, D., Talling, P.J., Watt, S.F.L., Cassidy, M., Jutzeler, M., Clare, M.A., Hunt, J.E., Manga, M., Gernon, T.M., Palmer, M.R., Hatter, S.J., Boudon, G., Endo, D., Fujinawa, A., Hatfield, R., Hornbach, M.J., Ishizuka, O., Kataoka, K., Le Friant, A., Maeno, F., McCanta, M., Stinton, A.J., 2016. The relationship between eruptive activity, flank collapse, and sea level at volcanic islands: A long-term (>1 Ma) record offshore Montserrat, Lesser Antilles. Geochemistry, Geophysics, Geosystems 17: 2591–2611.

Crandell, D.R., 1989. Gigantic debris avalanche of Pleistocene age from ancestral Mount Shasta volcano, California, and debris-avalanche hazard zonation. US Geological Survey Bulletin 1861, 32 pp.

Davidson, J., de Silva, S., 2000. Composite volcanoes. In: Sigurdsson, H., Houghton B.F., McNutt S.R., Rymer, H., Stix, J. (Eds.), Encyclopedia of volcanoes. Academic Press, San Diego, pp. 663-681.

Dávila Harris, P., Branney, M.J., Storey, M., 2011. Large eruption-triggered ocean-island landslide at Tenerife: Onshore record and long-term effects on hazardous pyroclastic dispersal. Geology, 39: 951-954.

Day, S.J., 1996. Hydrothermal pore fluid pressure and the stability of porous, permeable volcanoes. In: McGuire, W., Jones, A., Neuberg, J. (Eds.), Volcano instability on the Earth and other planets. Geological Society, London, Special Publications 110, pp.

77-93.
Day, S.J., Carracedi, J.C., Guillou, H., Gravestock, P., 1999a. Recent structural evolution of the Cumbre Vieja volcano, La Palma, Canary Islands: volcanic rift zone reconfiguration as a precursor to volcano flank instability. Journal of Volcanology and Geothermal Research 94: 135-167.
Day, S.J., Heleno da Silva, S.I.N., Fonseca, J.F.D.B., 1999b. A past giant lateral collapse and present-day flank instability of Fogo, Cape Verde Islands. Journal of Volcanology and Geothermal Research 94: 191-218.
Day, S., Llanes, P., Silver, E., Hoffmann, G., Ward, S., Driscoll, N., 2015. Submarine landslide deposits of the historical lateral collapse of Ritter Island, Papua New Guinea. Marine and Petroleum Geology, 67: 419-438.
de Silva, S., Lindsay, J.M., 2015. Primary volcanic landforms. In: Sigurdsson, H., Houghton B.F., McNutt S.R., Rymer, H., Stix, J. (Eds.), Encyclopedia of volcanoes. Elsevier, Amsterdam, pp. 273-297.
de Silva, S.L., Davidson, J.P., Croudace, I.W., Escobar, A., 1993. Volcanological and petrological evolution of volcan Tata Sabaya, SW Bolivia. Journal of Volcanology and Geothermal Research, 55: 305-335.
Deplus, C., Le Friant, A., Boudon, G., Komorowski, J.C., Villemant, B., Harford, C., Ségoufin, J., Cheminée, J.L., 2001. Submarine evidence for large-scale debris avalanches in the Lesser Antilles Arc. Earth and Planetary Science Letters, 192: 145-157.
Dóniz-Páez, J., 2015. Volcanic geomorphological classification of the cinder cones of Tenerife (Canary Islands, Spain). Geomorphology, 228: 432-447.
Dufresne, A., Davies, T.R., 2009. Longitudinal ridges in mass movement deposits. Geomorphology, 105: 171-181.
Eason, D.E., Sinton, J.M., Grönvold, K., Kurz, M.D., 2015. Effects of deglaciation on the petrology and eruptive history of the Western Volcanic Zone, Iceland. Bulletin of Volcanology, 77: 47.
Edgar, C.J., Wolff, J.A., Olin, P.H., Nichols, H.J., Pittari, A., Cas, R.A.F., Reiners, P.W., Spell, T.L., Martí, J., 2007. The late Quaternary Diego Hernandez Formation, Tenerife: Volcanology of a complex cycle of voluminous explosive phonolitic eruptions. Journal of Volcanology and Geothermal Research 160, 59-85.
Feeley, T.C., Davidson, J.P., Armendia, A., 1993. The volcanic and magmatic evolution of Volcán Ollagüe, a high-K, late Quaternary stratovolcano in the Andean Central Volcanic Zone. Journal of Volcanology and Geothermal Research, 54: 221-245.
Foroozan, R., Elsworth, D., Voight, B., Mattioli, G.S., 2010. Dual reservoir structure at Soufrière Hills Volcano inferred from continuous GPS observations and heterogeneous elastic modeling. Geophysical Research Letters, 37: L00E12.
Francalanci, L., Manetti, P., Peccerillo, A., 1989. Volcanological and magmatological evolution of Stromboli volcano (Aeolian Islands): the roles of fractional crystallization, magma mixing, crustal contamination and source heterogeneity. Bulletin of Volcanology, 51: 355-378.
Frey, F.A., Garcia, M.O., Wise, W.S., Kennedy, A., Gurriet, P., Albarede, F., 1991. The evolution of Mauna Kea volcano, Hawaii: petrogenesis of tholeiitic and alkalic basalts. Journal of Geophysical Research, 96: 14347-14375.
Frey, H.M., Lange, R.A., Hall, C.M., Delgado-Granados, H., 2004. Magma eruption rates constrained by 40Ar/39Ar chronology and GIS for the Ceboruco–San Pedro volcanic field, western Mexico. Geological Society of America Bulletin, 116: 259-276.
Galipp, K., Klügel, A., Hansteen, T.H., 2006. Changing depths of magma fractionation and stagnation during the evolution of an oceanic island volcano: La Palma (Canary

Islands). Journal of Volcanology and Geothermal Research, 155: 285-306.

Gardner, J.E., Rutherford, M.J., Carey, S.N., Sigurdsson, H., 1995. Experimental constraints on pre-eruptive water contents and changing magma storage prior to explosive eruptions of Mount St Helens volcano. Bulletin of Volcanology, 57: 1-17.

Gavrilenko, M., Ozerov, A., Kyle, P.R., Carr, M.J., Nikulin, A., Vidito, C., Danyushevsky, L., 2016. Abrupt transition from fractional crystallization to magma mixing at Gorely volcano (Kamchatka) after caldera collapse. Bulletin of Volcanology, 78: 1-28.

Geist, D., White, W.M., Albarede, F., Harpp, K., Reynolds, R., Blichert-Toft, J., Kurz, M.D., 2002. Volcanic evolution in the Galápagos: The dissected shield of Volcan Ecuador. Geochemistry, Geophysics, Geosystems, 3: 1061.

Gerbault, M., Cappa, F., Hassani, R., 2012. Elasto-plastic and hydromechanical models of failure around an infinitely long magma chamber. Geochemistry, Geophysics, Geosystems, 13: Q03009.

Germa, A., Lahitte, P., Quidelleur, X., 2015. Construction and destruction of Mont Pelée volcano: Volumes and rates constrained from a geomorphological model of evolution. Journal of Geophysical Research, 120: 1206-1226.

Germa, A., Quidelleur, X., Lahitte, P., Labanieh, S., Chauvel, C., 2011. The K/Ar Cassignol-Gillot technique applied to western Martinique lavas: A record of Lesser Antilles arc activity from 2Ma to Mount Pelée volcanism. Quaternary Geochronology, 6: 341-355.

Ginibre, C., Wörner, G., 2007. Variable parent magmas and recharge regimes of the Parinacota magma system (N. Chile) revealed by Fe, Mg and Sr zoning in plagioclase. Lithos, 98: 118-140.

Girina, O.A., 2013. Chronology of Bezymianny Volcano activity, 1956-2010. Journal of Volcanology and Geothermal Research 263: 22-41.

Glicken, H., 1996. Rockslide-debris avalanche of May 18, 1980, Mount St. Helens volcano, Washington. U.S. Geological Survey, Open-file Report 96-677, 90 pp.

Global Volcanism Program, 2013. Volcanoes of the World, v. 4.6.6. Venzke, E (ed.). Smithsonian Institution. https://dx.doi.org/10.5479/si.GVP.VOTW4-2013

Godoy, B., Clavero, J., Rojas, C., Godoy, E., 2012. Facies volcánicas del depósito de avalancha de detritos del volcán Tata Sabaya, Andes Centrales. Andean Geology, 39: 394-406.

Gorbach, N., Portnyagin, M., Tembrel, I., 2013. Volcanic structure and composition of Old Shiveluch volcano, Kamchatka. Journal of Volcanology and Geothermal Research, 263: 193-208.

Gorbach, N.V., Portnyagin, M.V., 2011. Geology and petrology of the lava complex of Young Shiveluch Volcano, Kamchatka. Petrology, 19: 134.

Grosfils, E.B., 2007. Magma reservoir failure on the terrestrial planets: Assessing the importance of gravitational loading in simple elastic models. Journal of Volcanology and Geothermal Research, 166: 47-75.

Grosse, P., Euillades, P.A., Euillades, L.D., van Wyk de Vries, B., 2014. A global database of composite volcano morphometry. Bulletin of Volcanology, 76: 1-16.

Gudmundsson, A., 2006. How local stresses control magma-chamber ruptures, dyke injections, and eruptions in composite volcanoes. Earth-Science Reviews, 79: 1-31.

Gudmundsson, A., 2012. Magma chambers: Formation, local stresses, excess pressures, and compartments. Journal of Volcanology and Geothermal Research, 237: 19-41.

Guillou, H., Carracedo, J.C., Day, S.J., 1998. Dating of the Upper Pleistocene–Holocene volcanic activity of La Palma using the unspiked K-Ar technique. Journal of Volcanology and Geothermal Research 86: 137-149.

Hall, M., Mothes, P., 2008. The rhyolitic–andesitic eruptive history of Cotopaxi volcano, Ecuador. Bulletin of Volcanology, 70: 675-702.

Hall, M.L., Robin, C., Beate, B., Mothes, P., Monzier, M., 1999. Tungurahua Volcano, Ecuador: structure, eruptive history and hazards. Journal of Volcanology and Geothermal Research, 91: 1-21.

Harford, C.L., Pringle, M.S., Sparks, R.S.J., Young, S.R., 2002. The volcanic evolution of Montserrat using 40Ar/39Ar geochronology. Geological Society, London, Memoirs, 21: 93-113.

Hildenbrand, A., Gillot, P.Y., Le Roy, I., 2004. Volcano-tectonic and geochemical evolution of an oceanic intra-plate volcano: Tahiti-Nui (French Polynesia). Earth and Planetary Science Letters, 217: 349-365.

Hildner, E., Klügel, A., Hansteen, T.H., 2012. Barometry of lavas from the 1951 eruption of Fogo, Cape Verde Islands: Implications for historic and prehistoric magma plumbing systems. Journal of Volcanology and Geothermal Research, 217: 73-90.

Hildreth, W., Fierstein, J., Lanphere, M.A., 2003. Eruptive history and geochronology of the Mount Baker volcanic field, Washington. Geological Society of America Bulletin, 115: 729-764.

Hildreth, W., Lanphere, M.A., 1994. Potassium-argon geochronology of a basalt-andesite-dacite arc system: The Mount Adams volcanic field, Cascade Range of southern Washington. Geological Society of America Bulletin, 106: 1413-1429.

Hildreth, W., Lanphere, M.A., Fierstein, J., 2003. Geochronology and eruptive history of the Katmai volcanic cluster, Alaska Peninsula. Earth and Planetary Science Letters, 214: 93-114.

Hill, D.P., Pollitz, F., Newhall, C., 2002. Earthquake-volcano interactions. Physics Today, 55: 41-47.

Hobden, B.J., Houghton, B.F., Davidson, J.P., Weaver, S.D., 1999. Small and short-lived magma batches at composite volcanoes: time windows at Tongariro volcano, New Zealand. Journal of the Geological Society, 156: 865-868.

Hora, J.M., Singer, B.S., Wörner, G., 2007. Volcano evolution and eruptive flux on the thick crust of the Andean Central Volcanic Zone: 40Ar/39Ar constraints from Volcán Parinacota, Chile. Geological Society of America Bulletin, 119: 343-362.

Hora, J.M., Singer, B.S., Wörner, G., Beard, B.L., Jicha, B.R., Johnson, C.M., 2009. Shallow and deep crustal control on differentiation of calc-alkaline and tholeiitic magma. Earth and Planetary Science Letters, 285: 75-86.

Hornig-Kjarsgaard, I., Keller, J., Koberski, U., Stadlbauer, E., Francalanci, L., Lenhart, R., 1993. Geology, stratigraphy and volcanological evolution of the island of Stromboli, Aeolian arc, Italy. Acta Vulcanologica, 3: 21-68.

Hunt, J.E., Wynn, R.B., Talling, P.J., Masson, D.G., 2013. Multistage collapse of eight western Canary Island landslides in the last 1.5 Ma: Sedimentological and geochemical evidence from subunits in submarine flow deposits. Geochemistry, Geophysics, Geosystems 14: 2159-2181.

Hunt, J.E., Talling, P.J., Clare, M.A., Jarvis, I., Wynn, R.B., 2014. Long-term (17 Ma) turbidite record of the timing and frequency of large flank collapses of the Canary Islands. Geochemistry, Geophysics, Geosystems 15: 3322-3345

Hunt, J.E., Cassidy, M., Talling, P.J., 2018. Multi-stage volcanic island flank collapses with coeval explosive caldera-forming eruptions. Scientific Reports, 8: 1146.

Hurwitz, D.M., Long, S.M., Grosfils, E.B., 2009. The characteristics of magma reservoir failure beneath a volcanic edifice. Journal of Volcanology and Geothermal Research, 188: 379-394.

Jicha, B.R., Laabs, B.J.C., Hora, J.M., Singer, B.S., Caffee, M.W., 2015. Early Holocene collapse of Volcán Parinacota, central Andes, Chile: Volcanological and paleohydrological consequences. Geological Society of America Bulletin, 127: 1681-

1688.
Jicha, B.R., Singer, B.S., 2006. Volcanic history and magmatic evolution of Seguam Island, Aleutian Island arc, Alaska. Geological Society of America Bulletin, 118: 805-822.
Johnson, R.W., 1987. Large-scale volcanic cone collapse: the 1888 slope failure of Ritter volcano, and other examples from Papua New Guinea. Bulletin of Volcanology, 49: 669-679.
Jull, M., McKenzie, D., 1996. The effect of deglaciation on mantle melting beneath Iceland. Journal of Geophysical Research, 101: 21815-21828.
Karlstrom, L., Dufek, J., Manga, M., 2010. Magma chamber stability in arc and continental crust. Journal of Volcanology and Geothermal Research, 190: 249-270.
Karlstrom, L., Wright, H.M., Bacon, C.R., 2015. The effect of pressurized magma chamber growth on melt migration and pre-caldera vent locations through time at Mount Mazama, Crater Lake, Oregon. Earth and Planetary Science Letters, 412: 209-219.
Karstens, J., Berndt, C., Urlaub, M., Watt, S.F.L., Micallef, A., Ray, M., Klaucke, I., Klaeschen, D., Kühn, M., Roth, T., Böttner, C., Schramm, B., Elger, J., Brune, S., 2019. From gradual spreading to catastrophic collapse – Reconstruction of the 1888 Ritter Island volcanic sector collapse from high-resolution 3D seismic data. Earth and Planetary Science Letters, in press.
Katsui, Y., Yamamoto, M., 1981. The 1741-1742 activity of Oshima-Ōshima volcano, north Japan. Journal of the Faculty of Science, Hokkaido University. Series 4, Geology and Mineralogy, 19: 527-536.
Kervyn, M., Ernst, G.G.J., van Wyk de Vries, B., Mathieu, L., Jacobs, P., 2009. Volcano load control on dyke propagation and vent distribution: Insights from analogue modeling. Journal of Geophysical Research, 114: B03401.
León, R., Somoza, L., Urgeles, R., Medialdea, T., Ferrer, M., Biain, A., García-Crespo, J., Mediato, J.F., Galindo, I., Yepes, J., 2017. Multi-event oceanic island landslides: New onshore-offshore insights from El Hierro Island, Canary Archipelago. Marine Geology, 393: 156-175.
Linde, A.T., Sacks, I.S., 1998. Triggering of volcanic eruptions. Nature, 395: 888.
Lipman, P.W., Rhodes, J.M., Dalrymple, G.B., 1990. The Ninole Basalt—implications for the structural evolution of Mauna Loa volcano, Hawaii. Bulletin of Volcanology, 53: 1-19.
Lohmar, S., López-Escobar, L., Moreno, H., 2005. Preliminary comparison between Antuco and Sierra Velluda Volcanoes (Southern Andes), extended abstract. ISAG, Barcelona, pp. 385-388.
Longpré, M.A., Chadwick, J.P., Wijbrans, J., Iping, R., 2011. Age of the El Golfo debris avalanche, El Hierro (Canary Islands): New constraints from laser and furnace 40Ar/39Ar dating. Journal of Volcanology and Geothermal Research, 203: 76-80.
Longpré, M.A., Troll, V.R., Walter, T.R., Hansteen, T.H., 2009. Volcanic and geochemical evolution of the Teno massif, Tenerife, Canary Islands: Some repercussions of giant landslides on ocean island magmatism. Geochemistry, Geophysics, Geosystems, 10: Q12017.
Maccaferri, F., Richter, N., Walter, T.R., 2017. The effect of giant lateral collapses on magma pathways and the location of volcanism. Nature Communications, 8: 1097.
Maclennan, J., Jull, M., McKenzie, D., Slater, L., Grönvold, K., 2002. The link between volcanism and deglaciation in Iceland. Geochemistry, Geophysics, Geosystems, 3: 1-25.
Manconi, A., Longpré, M.A., Walter, T.R., Troll, V.R., Hansteen, T.H., 2009. The effects of flank collapses on volcano plumbing systems. Geology, 37: 1099-1102.
Manga, M., Brodsky, E., 2006. Seismic triggering of eruptions in the far field: volcanoes and

geysers. Annual Review of Earth and Planetary Sciences, 34: 263-291.
Martí, J., Hurlimann, M., Ablay, G.J., Gudmundsson, A., 1997. Vertical and lateral collapses on Tenerife (Canary Islands) and other volcanic ocean islands. Geology, 25: 879-882.
Martínez, P., Singer, B.S., Moreno Roa, H., Jicha, B.R., 2018. Volcanologic and petrologic evolution of Antuco-Sierra Velluda, Southern Andes, Chile. Journal of Volcanology and Geothermal Research, 349: 392-408.
Masson, D.G., Harbitz, C.B., Wynn, R.B., Pedersen, G., Lövholt, F., 2006. Submarine landslides: processes, triggers and hazard prediction. Philosophical Transactions of the Royal Society A, 364: 2009-2039.
Masson, D.G., Le Bas, T.P., Grevemeyer, I., Weinrebe, W., 2008. Flank collapse and large-scale landsliding in the Cape Verde Islands, off West Africa. Geochemistry, Geophysics, Geosystems, 9: Q07015.
Masson, D.G., Watts, A.B., Gee, M.J.R., Urgeles, R., Mitchell, N.C., Le Bas, T.P., Canals, M., 2002. Slope failures on the flanks of the western Canary Islands. Earth-Science Reviews, 57: 1-35.
McGuire, W.J., 1996. Volcano instability: a review of contemporary themes. In: McGuire, W.J, Jones, A.P., Nueberg, J. (Eds.), Volcano instability on the Earth and other planets, Geological Society Special Publication 110, pp. 1-23.
McMurtry, G.M., Watts, P., Fryer, G.J., Smith, J.R., Imamura, F., 2004. Giant landslides, mega-tsunamis, and paleo-sea level in the Hawaiian Islands. Marine Geology, 203: 219-233.
Moore, J.G., Clague, D.A., Holcomb, R.T., Lipman, P.W., Normark, W.R., Torresan, M.E., 1989. Prodigious submarine landslides on the Hawaiian Ridge. Journal of Geophysical Research, 94: 17465-17484.
Muller, J.R., Ito, G., Martel, S.J., 2001. Effects of volcano loading on dike propagation in an elastic half-space. Journal of Geophysical Research, 106: 11101-11113.
Neri, M., Acocella, V., Behncke, B., 2004. The role of the Pernicana Fault System in the spreading of Mt. Etna (Italy) during the 2002–2003 eruption. Bulletin of Volcanology, 66: 417-430.
Oehler, J.F., Lénat, J.F., Labazuy, P., 2008. Growth and collapse of the Reunion Island volcanoes. Bulletin of Volcanology, 70: 717-742.
Pallister, J.S., Thornber, C.R., Cashman, K.V., Clynne, M.A., Lowers, H.A., Mandeville, C.W., Brownfield, I.K., Meeker, G.P., 2008. Petrology of the 2004-2006 Mount St. Helens lava dome-implications for magmatic plumbing and eruption triggering. In: Sherrod, D.R., Scott, W.E., Stauffer, P.H. (Eds.), A volcano rekindled: the renewed eruption of Mount St. Helens, 2004-2006. US Geological Survey Professional Paper 1750, pp. 647-702.
Paris, R., Coello Bravo, J.J., Martin González, M.E., Kelfoun, K., Nauret, F., 2017. Explosive eruption, flank collapse and megatsunami at Tenerife ca. 170 ka. Nature Communications, 8: 15246.
Paris, R., Ramalho, R.S., Madeira, J., Ávila, S., May, S.M., Rixhon, G., Engel, M., Brückner, H., Herzog, M., Schukraft, G., Perez-Torrado, F.J., Rodriguez-Gonzales, A., Carracedo, J.C., Giachetti, T., 2018. Mega-tsunami conglomerates and flank collapses of ocean island volcanoes. Marine Geology 395: 168-187.
Petrone, C.M., Braschi, E., Francalanci, L., 2009. Understanding the collapse-eruption link at Stromboli, Italy: a microanalytical study on the products of the recent Secche di Lazzaro phreatomagmatic activity. Journal of Volcanology and Geothermal Research 188: 315-332.
Pinel, V., Albino, F., 2013. Consequences of volcano sector collapse on magmatic storage zones: Insights from numerical modeling. Journal of Volcanology and Geothermal

Research, 252: 29-37.
Pinel, V., Jaupart, C., 2000. The effect of edifice load on magma ascent beneath a volcano. Philosophical Transactions of the Royal Society of London A, 358: 1515-1532.
Pinel, V., Jaupart, C., 2003. Magma chamber behavior beneath a volcanic edifice. Journal of Geophysical Research, 108: 2072.
Pinel, V., Jaupart, C., 2004. Magma storage and horizontal dyke injection beneath a volcanic edifice. Earth and Planetary Science Letters, 221: 245-262.
Pinel, V., Jaupart, C., 2005. Some consequences of volcanic edifice destruction for eruption conditions. Journal of Volcanology and Geothermal Research, 145: 68-80.
Pinel, V., Jaupart, C., Albino, F., 2010. On the relationship between cycles of eruptive activity and growth of a volcanic edifice. Journal of Volcanology and Geothermal Research, 194: 150-164.
Ponomareva, V.V., Melekestsev, I.V., Dirksen, O.V., 2006. Sector collapses and large landslides on Late Pleistocene - Holocene volcanoes in Kamchatka, Russia. Journal of Volcanology and Geothermal Research, 158: 117-138.
Presley, T.K., Sinton, J.M., Pringle, M., 1997. Postshield volcanism and catastrophic mass wasting of the Waianae Volcano, Oahu, Hawaii. Bulletin of Volcanology, 58: 597-616.
Pyle, D.M., 2000. Sizes of volcanic eruptions. In: Sigurdsson, H., Houghton, B.F., McNutt, S.R., Rymer, H., Stix, J. (Eds.), Encyclopedia of Volcanoes, Academic Press, pp. 263-269.
Rawson, H., Pyle, D.M., Mather, T.A., Smith, V.C., Fontijn, K., Lachowycz, S.M., Naranjo, J.A., 2016. The magmatic and eruptive response of arc volcanoes to deglaciation: Insights from southern Chile. Geology, 44: 251-254.
Reid, M.E., Sisson, T.W., Brien, D.L., 2001. Volcano collapse promoted by hydrothermal alteration and edifice shape, Mount Rainier, Washington. Geology, 29: 779-782.
Robin, C., Boudal, C., 1987. A gigantic Bezymianny-type event at the beginning of modern volcan Popocatepetl. Journal of Volcanology and Geothermal Research, 31: 115-130.
Robin, C., Eissen, J.P., Samaniego, P., Martin, H., Hall, M., Cotten, J., 2009. Evolution of the late Pleistocene Mojanda–Fuya Fuya volcanic complex (Ecuador), by progressive adakitic involvement in mantle magma sources. Bulletin of Volcanology, 71: 233-258.
Robin, C., Komorowski, J.C., Boudal, C., Mossand, P., 1990. Mixed-magma pyroclastic surge deposits associated with debris avalanche deposits at Colima volcanoes, Mexico. Bulletin of Volcanology, 52: 391-403.
Romagnoli, C., Casalbore, D., Chiocci, F.L., Bosman, A., 2009. Offshore evidence of large-scale lateral collapses on the eastern flank of Stromboli, Italy, due to structurally-controlled, bilateral flank instability. Marine Geology, 262: 1-13.
Ruprecht, P., Wörner, G., 2007. Variable regimes in magma systems documented in plagioclase zoning patterns: El Misti stratovolcano and Andahua monogenetic cones. Journal of Volcanology and Geothermal Research, 165: 142-162.
Rutherford, M.J., Devine, J.D., 2008. Magmatic Conditions and Processes in the Storage Zone of the 2004-2006 Mount St. Helens Dacite. In: Sherrod, D.R., Scott, W.E., Stauffer, P.H. (Eds.), A volcano rekindled: the renewed eruption of Mount St. Helens, 2004-2006. US Geological Survey Professional Paper 1750, pp. 703-725.
Samaniego, P., Barba, D., Robin, C., Fornari, M., Bernard, B., 2012. Eruptive history of Chimborazo volcano (Ecuador): A large, ice-capped and hazardous compound volcano in the Northern Andes. Journal of Volcanology and Geothermal Research, 221: 33-51.
Samper, A., Quidelleur, X., Lahitte, P., Mollex, D., 2007. Timing of effusive volcanism and

collapse events within an oceanic arc island: Basse-Terre, Guadeloupe archipelago (Lesser Antilles Arc). Earth and Planetary Science Letters, 258: 175-191.

Satake, K., 2007. Volcanic origin of the 1741 Oshima-Oshima tsunami in the Japan Sea. Earth, Planets and Space, 59: 381.

Satake, K., Kato, Y., 2001. The 1741 Oshima-Oshima Eruption: Extent and volume of submarine debris avalanche. Geophysical Research Letters, 28: 427-430.

Schaaf, P., Carrasco-Núñez, G., 2010. Geochemical and isotopic profile of Pico de Orizaba (Citlaltépetl) volcano, Mexico: Insights for magma generation processes. Journal of Volcanology and Geothermal Research, 197: 108-122.

Schindlbeck, J.C., Freundt, A., Kutterolf, S., 2014. Major changes in the post-glacial evolution of magmatic compositions and pre-eruptive conditions of Llaima Volcano, Andean Southern Volcanic Zone, Chile. Bulletin of Volcanology, 76: 830.

Scott, K.M., Macías, J.L., Naranjo, J.A., Rodríguez, S., McGeehin, J.P., 2001. Catastrophic debris flows transformed from landslides in volcanic terrains: mobility, hazard assessment, and mitigation strategies. U.S. Geological Survey Professional Paper 1630, 59 pp.

Shea, T., van Wyk de Vries, B., Pilato, M., 2008. Emplacement mechanisms of contrasting debris avalanches at Volcán Mombacho (Nicaragua), provided by structural and facies analysis. Bulletin of Volcanology, 70: 899-921.

Sherrod, D.R., Vallance, J.W., Espinosa, A.T., McGeehin, J.P., 2007. Volcán Barú—Eruptive History and Volcano-Hazards Assessment. US Geological Survey Open-File Report 1401: 33.

Siebert, L., 1984. Large volcanic debris avalanches: characteristics of source areas, deposits, and associated eruptions. Journal of Volcanology and Geothermal Research, 22: 163-197.

Siebert, L., Alvarado, G.E., Vallance, J.W., van Wyk de Vries, B., 2006. Large-volume volcanic edifice failures in Central America and associated hazards. In: Rose, W.I., Carr, G.J.S., Ewert, J.W., Patino, L.C., Vallance, J.W. (Eds.), Volcanic hazards in Central America. Geological Society of America Special Paper 412, pp. 1-26.

Siebert, L., Glicken, H., Ui, T., 1987. Volcanic hazards from Bezymianny- and Bandai-type eruptions. Bulletin of Volcanology, 49: 435-459.

Siebert, L., Kimberly, P., Pullinger, C.R., 2004. The voluminous Acajutla debris avalanche from Santa Ana volcano, western El Salvador, and comparison with other Central American edifice-failure events. In: Rose, W.I., Bommer, J.J., López, D.L., Carr, M.J., Major, J.J. (Eds.), Natural Hazards in El Salvador. Geological Society of America Special Paper 375, pp. 5-23.

Singer, B.S., Jicha, B.R., Harper, M.A., Naranjo, J.A., Lara, L.E., Moreno-Roa, H., 2008. Eruptive history, geochronology, and magmatic evolution of the Puyehue-Cordón Caulle volcanic complex, Chile. Geological Society of America Bulletin, 120: 599-618.

Singer, B.S., Thompson, R.A., Dungan, M.A., Feeley, T.C., Nelson, S.T., Pickens, J.C., Brown, L.L., Wulff, A.W., Davidson, J.P., Metzger, J., 1997. Volcanism and erosion during the past 930 ky at the Tatara–San Pedro complex, Chilean Andes. Geological Society of America Bulletin, 109: 127-142.

Smith, J.R., Wessel, P., 2000. Isostatic consequences of giant landslides on the Hawaiian Ridge. Pure and Applied Geophysics, 157: 1097-1114.

Staudigel, H., Clague, D.A., 2010. The geological history of deep-sea volcanoes: Biosphere, hydrosphere, and lithosphere interactions. Oceanography, 23: 115-129.

Stoopes, G.R., Sheridan, M.F., 1992. Giant debris avalanches from the Colima Volcanic Complex, Mexico: Implications for long-runout landslides (> 100 km) and hazard assessment. Geology, 20: 299-302.

Thouret, J.C., Finizola, A., Fornari, M., Legeley-Padovani, A., Suni, J., Frechen, M., 2001. Geology of El Misti volcano near the city of Arequipa, Peru. Geological Society of America Bulletin, 113: 1593-1610.

Thouret, J.C., Rivera, M., Wörner, G., Gerbe, M.C., Finizola, A., Fornari, M., Gonzales, K., 2005. Ubinas: the evolution of the historically most active volcano in southern Peru. Bulletin of Volcanology, 67: 557-589.

Tibaldi, A., 2001. Multiple sector collapses at Stromboli volcano, Italy: how they work. Bulletin of Volcanology, 63: 112-125.

Tibaldi, A., 2004. Major changes in volcano behaviour after a sector collapse: insights from Stromboli, Italy. Terra Nova, 16: 2-8.

Tibaldi, A., Corazzato, C., Kozhurin, A., Lagmay, A.F.M., Pasquarè, F.A., Ponomareva, V.V., Rust, D., Tormey, D., Vezzoli, L., 2008. Influence of substrate tectonic heritage on the evolution of composite volcanoes: Predicting sites of flank eruption, lateral collapse, and erosion. Global and Planetary Change, 61: 151-174.

Tormey, D., 2010. Managing the effects of accelerated glacial melting on volcanic collapse and debris flows: Planchon-Peteroa Volcano, Southern Andes. Global and Planetary Change, 74: 82-90.

Tormey, D.R., Frey, F.A., Lopez-Escobar, L., 1995. Geochemistry of the active Azufre—Planchon—Peteroa volcanic complex, Chile (35 15′ S): evidence for multiple sources and processes in a cordilleran arc magmatic system. Journal of Petrology, 36: 265-298.

Ui, T., 1983. Volcanic dry avalanche deposits--Identification and comparison with nonvolcanic debris stream deposits. Journal of Volcanology and Geothermal Research, 18: 135-150.

van Wyk de Vries, B., Self, S., Francis, P.W., Keszthelyi, L., 2001. A gravitational spreading origin for the Socompa debris avalanche. Journal of Volcanology and Geothermal Research, 105: 225-247.

Vezzoli, L., Renzulli, A., Menna, M., 2014. Growth after collapse: the volcanic and magmatic history of the Neostromboli lava cone (island of Stromboli, Italy). Bulletin of Volcanology, 76: 821.

Voight, B., Janda, R.J., Glicken, H., Douglass, P.M., 1983. Nature and mechanics of the Mount St. Helens rockslide-avalanche of 18 May 1980. Geotechnique, 33: 243-273.

Voight, B., Sousa, J., 1994. Lessons from Ontake-san: a comparative analysis of debris avalanche dynamics. Engineering Geology, 38: 261-297.

Voight, B., Komorowski, J.C., Norton, G.E., Belousov, A.B., Belousova, M., Boudon, G., Francis, P.W., Franz, W., Heinrich, P., Sparks, R.S.J., 2002. The 26 December (Boxing Day) 1997 sector collapse and debris avalanche at Soufrière Hills volcano, Montserrat. Geological Society of London Memoir, 21: 363-408.

Voight, B., Widiwijayanti, C., Mattioli, G., Elsworth, D., Hidayat, D., Strutt, M., 2010. Magma-sponge hypothesis and stratovolcanoes: Case for a compressible reservoir and quasi-steady deep influx at Soufrière Hills Volcano, Montserrat. Geophysical Research Letters 37, L00E05.

Wadge, G., 1982. Steady state volcanism: evidence from eruption histories of polygenetic volcanoes. Journal of Geophysical Research, 87: 4035-4049.

Wadge, G., Francis, P.W., Ramirez, C.F., 1995. The Socompa collapse and avalanche event. Journal of Volcanology and Geothermal Research, 66: 309-336.

Walter, T.R., Troll, V.R., Cailleau, B., Belousov, A., Schmincke, H.-U., Amelung, F., v.d. Bogaard, P., 2005. Rift zone reorganization through flank instability in ocean island volcanoes: an example from Tenerife, Canary Islands. Bulletin of Volcanology 67:

281-291.

Walter, T.R., Amelung, F., 2007. Volcanic eruptions following M≥ 9 megathrust earthquakes: Implications for the Sumatra-Andaman volcanoes. Geology, 35: 539-542.

Ward, S.N., Day, S., 2003. Ritter Island volcano - lateral collapse and the tsunami of 1888. Geophysical Journal International, 154: 891-902.

Watson, S., McKenzie, D., 1991. Melt generation by plumes: a study of Hawaiian volcanism. Journal of Petrology, 32: 501-537.

Watt, S.F.L., Pyle, D.M., Mather, T.A., 2009. The influence of great earthquakes on volcanic eruption rate along the Chilean subduction zone. Earth and Planetary Science Letters, 277: 399-407.

Watt, S.F.L., Pyle, D.M., Mather, T.A., 2013. The volcanic response to deglaciation: Evidence from glaciated arcs and a reassessment of global eruption records. Earth-Science Reviews, 122: 77-102.

Watt, S.F.L., Pyle, D.M., Naranjo, J.A., Mather, T.A., 2009. Landslide and tsunami hazard at Yate volcano, Chile as an example of edifice destruction on strike-slip fault zones. Bulletin of Volcanology, 71: 559-574.

Watt, S.F.L., Talling, P.J., Hunt, J.E., 2014. New insights into the emplacement dynamics of volcanic island landslides. Oceanography, 27: 46-57.

Watt, S.F.L., Talling, P.J., Vardy, M.E., Masson, D.G., Henstock, T.J., Hühnerbach, V., Minshull, T.A., Urlaub, M., Lebas, E., Le Friant, A., Berndt, C., Crutchley, G.J., Karstens, J., 2012. Widespread and progressive seafloor-sediment failure following volcanic debris avalanche emplacement: Landslide dynamics and timing offshore Montserrat, Lesser Antilles. Marine Geology, 323-325: 69-94.

Watt, S.F.L., Karstens, J., Micallef, A., Berndt, C., Urlaub, M., Ray, M., Desai, A., Sammartini, M., Klaucke, I., Böttner, C., Day, S., Downes, H., Kühn, M., Elger, J., 2019. From catastrophic collapse to multi-phase deposition: flow transformation, seafloor interaction and triggered eruption following a volcanic-island landslide. Earth and Planetary Science Letters, revised.

White, S.M., Crisp, J.A., Spera, F.J., 2006. Long-term volumetric eruption rates and magma budgets. Geochemistry, Geophysics, Geosystems, 7: Q03010.

Wolff, J.A., Grandy, J.S., Larson, P.B., 2000. Interaction of mantle-derived magma with island crust? Trace element and oxygen isotope data from the Diego Hernandez Formation, Las Cañadas, Tenerife. Journal of Volcanology and Geothermal Research, 103: 343-366.

Wooller, L., van Wyk de Vries, B., Murray, J.B., Rymer, H., Meyer, S., 2004. Volcano spreading controlled by dipping substrata. Geology, 32: 573-576.

Wörner, G., Harmon, R.S., Davidson, J., Moorbath, S., Turner, D.L., McMillan, N., Nye, C., Lopez-Escobar, L., Moreno, H., 1988. The Nevados de Payachata volcanic region (18°S/69°W, N. Chile). Bulletin of Volcanology, 50: 287-303.

Yamamoto, T., Nakamura, Y., Glicken, H., 1999. Pyroclastic density current from the 1888 phreatic eruption of Bandai volcano, NE Japan. Journal of Volcanology and Geothermal Research, 90: 191-207.

Yoshida, H., 2013. Decrease of size of hummocks with downstream distance in the rockslide-debris avalanche deposit at Iriga volcano, Philippines: similarities with Japanese avalanches. Landslides, 10: 665-672.

Zellmer, G.F., Hawkesworth, C.J., Sparks, R.S.J., Thomas, L.E., Harford, C.L., Brewer, T.S., Loughlin, S.C., 2003. Geochemical evolution of the Soufriere Hills volcano, Montserrat, Lesser Antilles volcanic arc. Journal of Petrology, 44: 1349-1374.

Zernack, A.V., Cronin, S.J., Bebbington, M.S., Price, R.C., Smith, I.E.M., Stewart, R.B.,

Procter, J.N., 2012. Forecasting catastrophic stratovolcano collapse: A model based on Mount Taranaki, New Zealand. Geology, 40: 983-986.
Zernack, A.V., Cronin, S.J., Neall, V.E., Procter, J.N., 2011. A medial to distal volcaniclastic record of an andesite stratovolcano: detailed stratigraphy of the ring-plain succession of south-west Taranaki, New Zealand. International Journal of Earth Sciences, 100: 1937-1966.
Zernack, A.V., Procter, J.N., Cronin, S.J., 2009. Sedimentary signatures of cyclic growth and destruction of stratovolcanoes: a case study from Mt. Taranaki, New Zealand. Sedimentary Geology, 220: 288-305.

Table 1: Theoretical impacts of sector collapse on an upper crustal liquid magma body[a].

Sector collapse type		**Pressure parameters (*P*) (Fig. 3)[b] and impact**			
		$P_{r(f)} < P_{r(i)}$		$P_{r(f)} > P_{r(i)}$	
Eruption-related collapse	*incipient eruption:*	if $P_{m(f)} > P_{r(f)}$	if $P_{c(f)} < P_{m(f)} < P_{r(f)}$	if $P_{c(f)} < P_{m(f)}$	if $P_{c(f)} < P_{m(f)}$
		larger eruption	smaller eruption		stalled eruption
	subsequent eruptions:	shorter time to eruption, higher rate		longer time to eruption, lower rate	
Eruptible magma present		if $P_{m(f)} > P_{r(f)}$ triggered eruption	otherwise, shorter time to eruption, higher rate	longer time to eruption, lower rate	
No eruptible magma		when eruptible magma forms, eruption favoured relative to pre-collapse conditions		when eruptible magma forms, eruption impeded relative to pre-collapse conditions	

[a] cf. Pinel and Albino (2013)

[b] Subscript *(i)* refers to pre-collapse conditions; *(f)* refers to post-collapse conditions

Table 2: Summary of historical sector collapses (volumes >1 km³)[a].

Location	**Date (A.D.)**	**Collapse volume (km³)**	**Preceding repose interval**	**Precursory activity**	**Post-collapse activity**
Oshima-Oshima, Japan	1741	2.5[b]	~1500 years	~10 days of explosive eruptions	Strong explosive eruption accompanying collapse; ~9 months intense activity; minor sporadic activity to 1790; no subsequent eruption
Ritter Island, Papua New Guinea[c]	1888	4.2; 2.4[d]	1-3 years?; frequent minor explosive eruptions	Uncertain	Compositionally bimodal post-collapse eruption, including an evolved pumiceous component not known from any other Ritter samples. Extent of eruption-associated turbidite, immediately overlying collapse deposits, suggests a powerful submarine explosive eruption triggered by collapse. Smaller subsequent eruptions have built a submarine scoria cone within the scar, compositionally distinct from pre-collapse samples and involving both more mafic and more evolved components.
Bandai, Japan	1888	0.5[e]	No magmatic activity for ~25 kyr; phreatic explosions in 1808	1 week of minor seismicity; event triggered by M5 earthquake	Immediate strong phreatic eruption. No subsequent activity.
Shiveluch, Kamchatka	1964	1.15	Preceding eruption in 1946-50; frequent prior activity (effusive and explosive)	Seismicity over 10 months, accelerating before collapse	Immediate phreatic explosion; Plinian eruption within minutes, but no directed blast. Broadly continuous extrusion with explosions from 1980 to present.
Mount St.	1980	2.3-2.5	Last eruption	2 months of	Immediate lateral blast and Plinian

Helens, U.S.A.	~1857; frequent prior activity	increasing seismicity, slope deformation and phreatic explosions.	explosive eruption, followed by lava-dome extrusion; subsequent phases of dome extrusion.

[a] Data from Global Volcanism Program (2013) and: Oshima-Oshima (Katsui and Yamamoto, 1981; Satake and Kato, 2001; Satake, 2007); Ritter (Johnson, 1987; Day et al., 2015; Karstens et al., 2019; Watt et al., 2019); Bandai (Yamamoto et al., 1999; Yoshida, 2013); Shiveluch (Belousov, 1995; Ponomareva et al., 2006); Mount St. Helens (Voight et al., 1983; Glicken, 1996).

[b] The subaerial collapse scar suggests a much smaller volume (0.4 km^3); the larger volume is based on relatively limited bathymetry, but is consistent with tsunami observations (Satake and Kato, 2001).

[c] The base of the scar is several hundred metres below sea-level, meaning that replacement by seawater partially compensates for the mass-removal associated with collapse.

[d] Volumes based on reconstructions in Day et al. (2015) and Karstens et al. (2019) respectively.

[e] An earlier quoted volume of 1.4 km^3 is disputed by later authors, whose topographic reconstructions suggest a volume of $\leq$0.5 km^3 (cf. Yoshida, 2013).

Table 3: Sector collapses from arc volcanoes associated with an identified change in magma composition or eruptive behaviour[a].

Volcano	Collapse name	Age (ka)	Volume (km^3)	Observations: chemical and petrological	Observations: eruption rate and style	Sources
Shiveluch, Kamchatka	Old Shiveluch	16-10	~30	A greater predominance of more evolved (intermediate) magmas post-collapse. Evolved compositions are broadly similar pre- and post-collapse, but mafic compositions are distinct (pre-collapse have lower Mg#, higher Fe, Ti, and distinct trace element compositions (e.g. Cr, V)).	Frequent large explosive eruptions over 3kyr post collapse, then infrequent. Pre-collapse edifice very large but structurally stable; post-collapse marked by frequent repetitive small collapses. Increases in magma viscosity post-collapse; a dominance of lava domes over flows, leading to a steeper and possibly less stable edifice.	Belousov et al. 1999; Gorbach et al., 2013
Nevado de Colima, Mexico		18.5	6-12	Collapse deposit overlain by PDC deposits with mixed juvenile material, including the most mafic products known from the volcano. Petrological observations (reaction rims, resorption) and textural evidence of mixing in juvenile material indicate mixing of mafic and felsic magmas prior to eruption. Later lavas (basaltic andesites) are compositionally similar to those preceding collapse.		Robin et al., 1990; Stoopes and Sheridan, 1992; Capra et al., 2002
Fuego de Colima, Mexico		early- to mid-Holocene	~10	Collapse preceded by dacites, but subsequent PDCs contain basaltic andesite juvenile material, and andesites dominate subsequent cone rebuilding.	Thick andesite lava flows precede collapse; explosive andesitic eruptions, at higher frequency for ~1 kyr after collapse, have dominated subsequent cone building.	Robin et al., 1990; Stoopes and Sheridan, 1992; Capra et al., 2002
Orizaba, Mexico	Torrecillas/ Jamapa	210	~25	Poorly resolved shift in dominant mineral assemblage from pyroxene andesite to hornblende andesite in pre- and post-collapse units.		Carrasco-Núñez et al., 2006; Schaaf and Carrasco-Núñez, 2010
Soufrière Hills, Montserrat	Deposit 2/South Soufrière Hills	130	6-10	Sharp departure from pre-collapse two-pyroxene andesites to subsequent basaltic volcanism in the South Soufrière Hills episode. Younger andesites are petrographically distinct (hornblende-phyric) from pre-collapse andesites.	Available dates suggest elevated eruption rates and a duration of less than a few thousand years for the South Soufrière Hills episode.	Watt et al., 2012; Cassidy et al., 2015a
Conil/Pelée, Martinique	Le Prêcheur, D1	126	15	Collapse closely bracketed by two extremely similar lavas (possible extrusion-driven collapse, or post-collapse eruption driven by reservoir unloading).		Germa et al., 2011, 2015; Boudon et al.,

				Collapse marks the end of the Conil complex (andesitic); subsequent early stages of Pelee complex dominated by basaltic andesite.		2013
Pelée, Martinique	St Pierre, D2	~32	9	Collapse preceded by acid andesites and followed by basaltic andesite eruptions from ~32-27 ka, the system then returning to acid andesite eruptions from ~22.5 ka.	Increased eruption frequency in 5 kyr post-collapse period (based on marine tephra deposits) and change in predominant style from dome-forming to explosive behaviour.	Boudon et al., 2013; Germa et al., 2015
Tungurahua, Ecuador	Tungurahua II	3	6	Collapse of the andesitic TII edifice was followed by extrusion of mineralogically unusual dacite lavas (ol, cpx, opx and amph-phyric) before a 700-yr pause in volcanism, followed by eruption of homogeneous basaltic andesites (2.3-1.4 ka), distinct from pre-collapse magma compositions. Eruptions since 1.2 ka include more evolved compositions. Collapse of the TI replicates this broad pattern.	Post-collapse dacite lavas are unusually extensive (6 km flow lengths). Subsequent cone rebuilding activity at high eruptive flux (1.5 km^3/kyr).	Hall et al., 1999
Chimborazo, Ecuador	Riobamba	65-60	10-12	Collapse marks a permanent shift in magma chemistry; post-collapse rocks are more mafic, lack amphibole as a phenocryst phase, and are enriched in Mg, K and some trace elements (e.g. Rb, Th) relative to pre-collapse.	Voluminous and homogeneous andesitic lava flows (1-1.5km^3) erupted post-collapse. Large volume of flows notable in long term history of volcano.	Samaniego et al., 2012
Tata Sabaya, Bolivia		~6	6	Post-collapse thick lava domes and flows, all of very similar composition. Similar compositions throughout history of volcano, but two possibly early post-collapse domes contain inclusions more mafic than any other known products at the volcano. Other post-collapse lavas are more porphyritic and more evolved, but the relative timing of post-collapse eruptions is poorly constrained.		de Silva et al., 1993; Godoy et al., 2012
Parinacota, Chile	Parinacota	9	6	Post-collapse magmas more mafic than pre-collapse rocks and include the most mafic products known at the volcano (from flank vents), although these fall on a longer term trend to more mafic compositions. Post-collapse magmas geochemically consistent with rapid crustal transit and limited upper-crustal storage, in contrast with pre-collapse rocks. Phenocryst assemblage changes from hornblende-andesite to post-collapse two-pyroxene (Hbl absent)	Very high eruptive flux (up to 10 km^3/kyr) for up to two thousand years post-collapse. Rapid regrowth has buried collapse scar.	Wörner et al., 1988; Hora et al., 2007, 2009; Jicha et al., 2015

				assemblages.		
Planchón, Chile	Rio Teno	11	4-5	Basaltic rocks predominate at Planchón, but these evolved pre-collapse to basaltic andesite, with evidence for upper crustal storage. Post-collapse compositions revert to more mafic basalts, similar to earlier Planchón lavas.	Post-collapse vent migrated to focus within centre of collapse scar (cf. Stromboli). Higher proportion of pyroclastic material (i.e. explosive activity) relative to pre-collapse volcano.	Tormey et al., 1995; Tormey, 2010
San Pedro (Tatara – San Pedro), Chile		mid-Holocene	~4	Collapse was followed by eruption of ~1 km^3 compositionally variable silicic lavas, containing basaltic and gabbroic inclusions, and an associated explosive deposit. These lavas are interpreted as representing eruption from a zoned storage system; they are petrologically (e.g. amphibole-phyric) and chemically (Sr isotope and trace element signatures) distinctive from pre-collapse basaltic andesite and andesites, and younger basaltic andesites, which are also distinct from each other.	The composite post-collapse flow is relatively voluminous, with a total volume of 0.8 km^3 contrasting with 0.2 km^3 total volume for subsequent Holocene summit flows.	Costa and Singer, 2002
Antuco, Chile		6	5	Pre-collapse rocks span basalts to dacites; the earliest post-collapse lavas are basaltic andesite, but followed by more mafic explosive and effusive eruptions that have infilled much of the collapse scar and persisted for the rest of the Holocene.	Debris avalanche overlain by two unusually voluminous lava flows, compositionally identical, and distinct from the more mafic units that have dominated subsequent activity, and have been erupted at a higher flux than pre-collapse magmas.	Lohmar et al., 2005; Martínez et al., 2018; Watt, unpublished data
Stromboli, Italy	Upper Vancori	14	1.4-3.1	Pre-collapse latite to trachyte compositions are followed by relatively monotonous highly porphyritic shoshonites, the most potassic rocks known at the volcano and much more basic than any rocks from the preceding period. More evolved biotite shoshonites, consistent with fractional crystallisation of preceding magmas, erupt towards the end of the period (6 ka), implying re-establishment of upper crustal storage.	Effusive eruptions dominate the Neostromboli period (13-6 ka) at a higher eruptive flux than the pre-collapse period.	Francalanci et al., 1989; Hornig-Kjarsgaard et al., 1993; Tibaldi, 2001, 2004; Romagnoli et al., 2009; Vezzoli et al., 2014
Stromboli, Italy	Neostromboli	6	~1	The collapse-associated Secche di Lazzaro deposits share petrographic and geochemical characteristics with late-Neostromboli evolved shoshonites, but are mineralogically and compositionally heterogeneous, consistent with decompression (i.e. collapse) driven	Collapse associated Secche di Lazzaro deposits represent the most intense explosive activity of the past 6 kyr, suggestive of collapse-driven decompression of the shallow plumbing	Bertagnini and Landi, 1996; Tibaldi, 2001; Petrone et al., 2009; Vezzoli et

			disruption of the shallow reservoir. No evidence of fresh mafic input prior to collapse. Subsequent activity shifts to basaltic-shoshonitic magmas, continuing across younger small sector collapses.	and hydrothermal system. Younger activity dominated by strombolian behaviour.	al., 2014
Ritter Island, Papua New Guinea	AD 1888	2.4-4.2	See Table 2.	See Table 2.	Day et al., 2015; Karstens et al., 2019; Watt et al., 2019

[a] Additional examples with more limited data include Santa Ana, El Salvador (Siebert et al., 2004), Ollagüe, Chile/Bolivia (Feeley et al., 1993), St Lucia and Martinique (Boudon et al., 2013) and Guadeloupe (Samper et al., 2007), as discussed in the text.

Table 4: Sector collapses from intraplate ocean-island volcanoes associated with an identified change in magma composition or eruptive behaviour.

Island / volcano	Collapse name	Age (ka)	Volume (km^3)	Observations: chemical and petrological	Observations: eruption rate and style	Sources
Tenerife, Canary Islands[a]	Icod	175	80-150	Large-volume phonolitic explosive eruptions preceded event, but may also have accompanied or been triggered by latter stages of failure (Abrigo ignimbrite). Subsequent lavas infilling the base of the scar are mafic, transitioning to more evolved compositions over tens of kyr, with eventual establishment of shallow magma storage and growth the phonolitic Teide complex.	Mafic lavas emplaced at elevated rate over 10 kyr post-collapse period, with broadly exponential subsequent decline in output rates associated with increasing prevalence of more evolved compositions.	Ablay and Hürlimann, 2000; Masson et al., 2002; Carracedo et al., 2007; Boulesteix et al., 2012; Paris et al., 2017; Hunt et al., 2018
Tenerife, Canary Islands[b]	Micheque	830		Early post-collapse rocks are mafic ankaramites and plagioclase basalts. Later eruptions of intermediate and evolved (trachytes) magmas, within the collapse scar, suggest that centralised volcanism within the scar promoted shallow magma storage and differentiation, across a 300 kyr period.	Infilling of the collapse scar suggests high eruption rates of post-collapse volcanism (particularly in the initial stages), focused within the scar and promoting shallow magma storage and differentiation.	Carracedo et al., 2011
Tenerife, Canary Islands	Teno massif, two unnamed landslides	6100-5900	>20-25 each	The youngest pre-collapse rocks include the most silicic and least magnesian lavas from the shield stratigraphy, while rocks above the collapse unconformities are notably mafic, marking a sharp transition. The pattern is repeated for each landslide. Dense, crystal-rich ankaramites are also notably frequent in the immediate post-collapse sequences.	Lapilli-tuffs in post-collapse breccia sequences suggest explosive eruptions following collapse (derived from the disrupted shallow plumbing system), anomalous in the lava-dominated shield.	Longpré et al., 2009
La Palma, Canary Islands	Cumbre Nueva	560	95	Post-collapse growth of Bejenado volcano across a shallowing trend (~25-18 km) and showing evidence of increasing differentiation and reduced magma supply rates through time. Storage depths distinct from pre-collapse magmas, suggesting development of a distinct post-collapse plumbing system.	Elevated growth rates in early post-collapse stages.	Guillou et al., 1998; Masson et al., 2002; Galipp et al., 2006
El Hierro, Canary Islands	El Golfo	87-39	247	Pre-collapse units include Mg-poor trachytes (~60 wt% SiO_2), but evolved compositions are absent in the post-collapse stratigraphy, dominated by dense, crystal-rich and high-MgO basanites (mean of 44 wt% SiO_2).		Manconi et al., 2009; Longpré et al., 2011; León et al., 2017

Fogo, Cape Verde	Monte Amarelo	123-62	130-160	Early post-collapse magmas stored at lower depths than immediately preceding magmas (although all depths are uppermost mantle, with no evidence for prolonged crustal storage). Later eruptions span broader and shallower pressure ranges, suggesting increasing complexity of plumbing system established upon regrowth.	Post-collapse vent migration is consistent with modified magma ascent pathways and development of a distinct plumbing system.	Day et al., 1999b; Amelung and Day, 2002; Hildner et al., 2012; Maccaferri et al., 2017
Tahiti	N. landslide	870	>500	Sharp shifts in La/Yb, and Sr and Nd isotope ratios in post-collapse magmas are consistent with increased decompression melting, with further isotopic evolution and transition to silica-undersaturated compositions suggesting reduced melting upon regrowth.	90 kyr post-collapse period of elevated output (~5 km^3/kyr), interpreted as arising from increased mantle melt fraction. Gradual reduction in productivity and output rate upon regrowth.	Hildenbrand et al., 2004
Volcan Ecuador, Isabela, Galapagos		<100	unknown	A high proportion of post-collapse magmas with elevated Mg# and in some cases lying on distinct trace-element trends (shifted to higher Mg#) relative to the more consistent compositions of pre-collapse lavas.	Post-collapse shift in dominant vent locations, suggesting either bypassing of formerly dominant shallow reservoir, or destruction of this reservoir following collapse.	Geist et al., 2002
Waianae, Oahu, Hawaii[c]	Waianae slump	2980	up to 6100	Collapse separates Palehua (older) and Kolekole (younger) members, with Palehua showing temporal evolution towards lower degrees of partial melting (based on Nb/Zr), and the post-collapse onset of Kolekole sharply reversing this trend, being comparable to early Palehua lavas. Higher Mg contents and bulk chemistry suggest Kolekole lavas evolved at greater depths than Palehua, fractionating ol + cpx, with lower overall extents of fractionation than Palehua.		Presley et al., 1997

[a] An older (but potentially much smaller volume) collapse to the south of the caldera may have been eruption triggered (Dávila Harris et al., 2011; Paris et al., 2017).
[b] Other collapses on N.E. rift zone (Orotava, Güímar) occurred at a similar time and after the Micheque collapse, but the strongest evidence of a post-collapse control on subsequent rift volcanism is within the infilled Micheque collapse scar (Carracedo et al., 2011). .
[c] More limited evidence of post-collapse rejuvenated volcanism exists for other Hawaiian volcanoes (cf. Presley et al., 1997), while post-collapse plumbing system modification, and possible chemical changes and an episode of phreatomagmatic activity, were associated with the SW Mauna Loa landslides (Lipman et al., 1990).

Figure 1

Example morphologies of volcanoes affected by sector collapse. **A**: Oblique view of Mount St Helens, USA (image: NASA Earth Observatory), showing the approximate distribution of the landslide mass (Glicken, 1996) following the 1980 sector collapse. The distance across the collapse amphitheatre is 2 km. The deposit volume of 2.5 km^3 was distributed up to 29 km from the volcano (Glicken, 1996). **B**: Gradient-shaded bathymetry of Ritter Island, Papua New Guinea (image: Christoph Böttner), site of the largest historical sector collapse, in 1888, showing the submerged island morphology (the shallowest edifice and subaerial remnant is not shown). The collapse was approximately twice the volume of that at Mount St. Helens (Day et al., 2015). **C**: Scale cross-sections (without vertical exaggeration) through Socompa, Chile (one of the largest known subaerial sector collapses; Wadge et al., 1995) and Ritter Island (Ward and Day, 2003), both composite volcanoes in arc settings, and El Hierro, Canary Islands (Masson et al., 2002), one of the youngest examples of a large-scale flank landslide on an oceanic intraplate volcanic island. The pre-failure surfaces are conjectural.

Figure 2

A summary of documented sector collapses (>1 km^3). **A**: Global distribution of known examples, divided by tectonic setting. **B**: Relative proportions of sector collapse volumes across different tectonic settings (for events where specific volume estimates are available). Most subduction-zone collapses are <5 km^3, and the very largest collapses are all from intraplate ocean islands.

Figure 3

A theoretical framework for investigating the effects of edifice loading on magma chamber pressure, dyke formation and eruption rate (cf. Pinel et al., 2010). **A**: An edifice load ($\rho_E gh$) affects the stress field around an upper crustal liquid cavity, characterised by a pressure P_m, and connected to a deeper source with pressure P_S and density ρ_M. P_r describes the critical pressure for magma chamber rupture and dyke formation, and P_c the pressure at which this dyke will close. Any change in edifice load (depicted in red) will alter P_m, P_r and P_c. **B**: The rate of pressurisation of a shallow cavity connected to a deeper source depends on the pressure difference between the two (shown by the black curve), predicting a constant eruption rate under any particular set of conditions. If P_r is relatively low (condition 1), then replenishment of the upper chamber (following the pressure drop to P_c) will be relatively rapid. At higher P_r (condition 2), a longer pressurisation time results in a lower eruption rate. **C**: As an edifice load increases, P_r falls to a minimum and then increases with further edifice loading, with the eruption rate therefore following an opposite pattern. Sector collapse results in an instantaneous reduction in edifice load. This may either favour (condition 1) or impede (condition 2) subsequent eruptions, depending on the impact of unloading on P_r.

Figure 4

Long-term eruptive flux at well studied composite arc volcanoes. The main graph shows estimates of eruptive flux through time (<400 ka) compiled from detailed field studies at thirteen volcanoes (Hildreth and Lanphere, 1994; Singer et al., 1997, 2008; Hobden et al., 1999; Davidson and de Silva, 2000; Thouret et al., 2001; Hildreth et al., 2003a, 2003b; Frey et al., 2004; Bacon and Lanphere, 2006; Jicha and Singer, 2006; Hora et al., 2007, 2009; Samaniego et al., 2012). Relatively short episodes of heightened output are often interspersed with longer, quieter periods. The average of all datasets is shown as a red line (with shaded upper and lower quartiles). The inset graph shows literature estimates of eruptive flux against the duration of the estimate (data from Wadge, 1982; Hall et al., 1999; Thouret et al., 2001, 2005; White et al., 2006; Singer et al., 2008; Samaniego et al., 2012; Zernack et al., 2012), showing that decreasing temporal resolution leads to lower apparent flux.

Figure 5

Examples of anomalous post-collapse eruptions, interpreted as representing collapse-driven disruption of a pre-existing magma reservoir. A: Post-collapse lava flows at Antuco, Chile, directly overlying the mid-Holocene sector collapse deposit. The two lavas have near identical compositions, and are less mafic than the basalts that have dominated subsequent cone rebuilding in the collapse scar. These lavas are unusually voluminous and extensive in the context of both older and younger activity. B: Compositionally anomalous post-collapse products at Nevado de Colima, Mexico (Robin et al., 1987, 1990) and San Pedro, Chile (Costa and Singer, 2002). In both cases debris avalanche deposits are directly overlain by units that span a wide bulk compositional range, and in the case of San Pedro also have a distinctive phenocryst assemblage relative to both pre- and post-collapse products. Post-collapse lavas at Tungurahua, Ecuador, provide a comparable example (Hall et al., 1999).

Figure 6

Post-collapse shifts to more mafic magma compositions (highlighted by bulk MgO and SiO_2 compositions) for collapses at Soufrière Hills, Montserrat (Zellmer et al., 2003; Cassidy et al., 2012, 2015a), Pelée, Martinique (Boudon et al., 2013), Stromboli, Italy (Hornig-Kjarsgaard et al., 1993; Vezzoli et al., 2014), and Parinacota, Chile (Hora et al., 2009). Data are plotted at the same timescale and demonstrate the data gaps and differences in temporal resolution that hinder inter-volcano comparisons and reconstructions of eruptive behaviour associated with prehistoric sector collapses. When specific ages are unavailable, the stratigraphic intervals of data are indicated by vertical arrows. Soufrière Hills and Pelée returned to eruption of more evolved compositions, comparable but not identical to pre-collapse rocks. Further examples of more mafic magmatism in post-collapse cone-building episodes are provided in Table 3.

Figure 7

Persistent shifts in bulk magma compositions following sector collapse, at Shiveluch, Kamchatka (Gorbach and Portnyagin, 2011; Gorbach et al., 2013) and Chimborazo, Ecuador (Samaniego et al., 2012). The sharp nature of these shifts, replicated at several other volcanoes, are interpreted as indicating that the post-collapse reservoir is discrete (compositionally, geometrically or thermally) from the preceding system, with resultant changes in the relative crustal influences on erupted magma compositions.

Figure 8

A conceptual model of the impact of large-volume sector collapse at an arc volcano. The top panel depicts the pre-collapse state, with a magma reservoir in equilibrium with the surface load. Short term post-collapse behaviour is dependent on the presence of eruptible magma, which may be destabilised by the surface mass redistribution. Cone rebuilding is promoted by subsequent ascent of deeper mafic magmas, which may reach the surface with little modification. Longer-term regrowth promotes upper crustal storage and a return to more evolved compositions, but with a plumbing system that is spatially and temporally distinct from the pre-collapse reservoir.

Figure 9

Sector collapse and magmatic processes on Tenerife, Canary Islands. The map shows three morphologically prominent collapse scars, the youngest of which is the Icod landslide (~175 ka; Boulesteix et al., 2012), as well as the location of the Micheque collapse scar (Carracedo et al., 2011). Mafic vent sites (from Dóniz-Páez, 2015) highlight the rift zone structure of the island. More evolved magmas only erupt in the central region (Ablay et al., 1998), which is also the location of the Cañadas caldera structure, and inferred to mark a long-lived upper crustal magma reservoir. The central panel shows reconstructed eruption rates in the caldera region following the Icod collapse, and the right panel shows bulk rock MgO and K_2O contents for the same area (based on extrapolated ages, and both derived from the lava stratigraphy in Boulesteix et al. (2012)). This highlights a sharp-shift to mafic compositions following the Abrigo ignimbrite eruptions (composition from Wolff et al. (2000)), temporarily elevated and then declining eruption rates, and a trend towards more evolved compositions as upper-crustal magma storage is re-established over a ~150 kyr period.

Figure 10
Long-term magmatic trends at various ocean islands indicative of a direct collapse-driven influence on magma plumbing systems. The left panel shows calculated storage depths (from clinopyroxene-melt barometry) for eruptive units from La Palma, Canary Islands (Galipp et al., 2006) and Fogo, Cape Verde Islands (Hildner et al., 2012), highlighting gradual shallowing trends over ~100 kyr time periods, with a shift to higher pressures following sector collapse. The right panel shows changes in trace element chemistry of lavas on Tahiti (Hildenbrand et al., 2004, plotting only lavas with a differentiation index <30), either side of the major ~870 ka collapse. A compositional shift coincides closely with collapse, and suggests an interruption of long-term evolutionary trends. This is interpreted by Hildenbrand et al. (2004) as reflecting a relationship between loading, collapse, and mantle partial melting, with a collapse-driven increase in melt fraction.

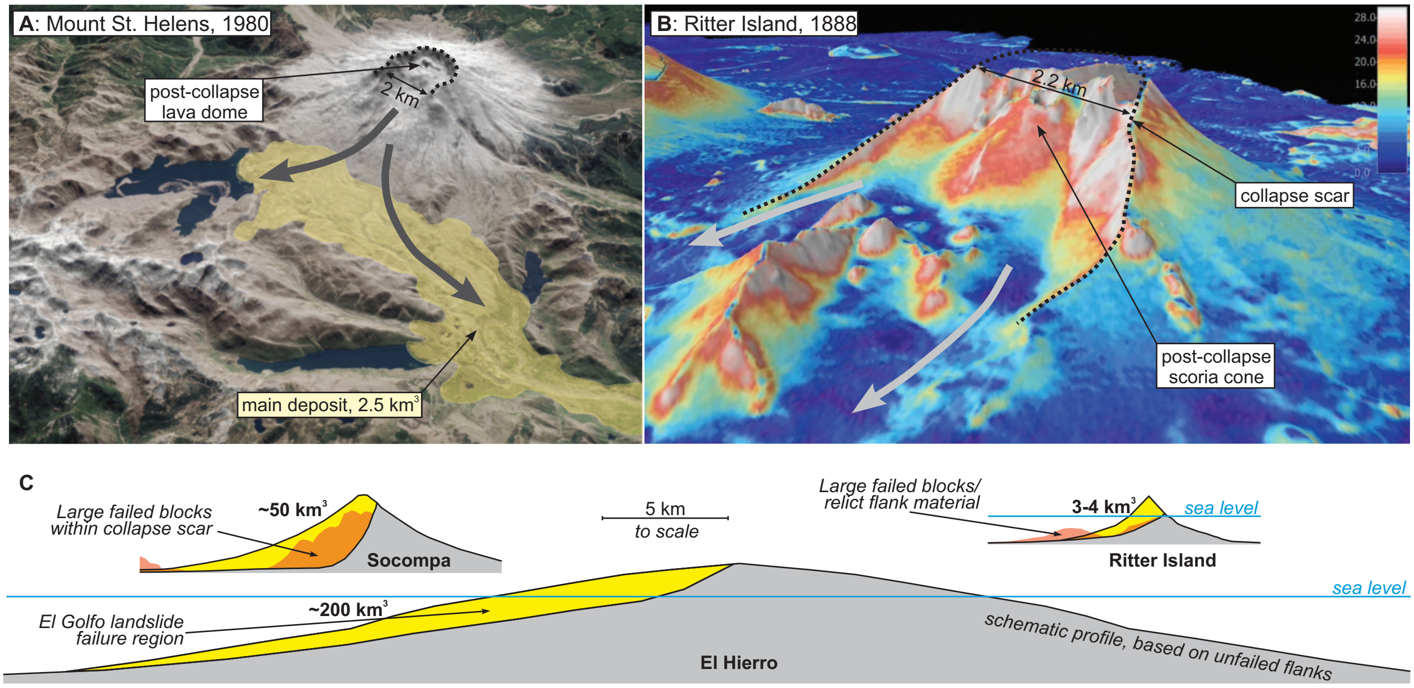

A: Mount St. Helens, 1980
post-collapse lava dome
2 km
main deposit, 2.5 km^3
B: Ritter Island, 1888
2.2 km
collapse scar
post-collapse scoria cone
C
Large failed blocks within collapse scar
~50 km^3
Socompa
5 km
to scale
Large failed blocks/ relict flank material
3-4 km^3
sea level
Ritter Island
sea level
El Golfo landslide failure region
~200 km^3
schematic profile, based on unfailed flanks
El Hierro

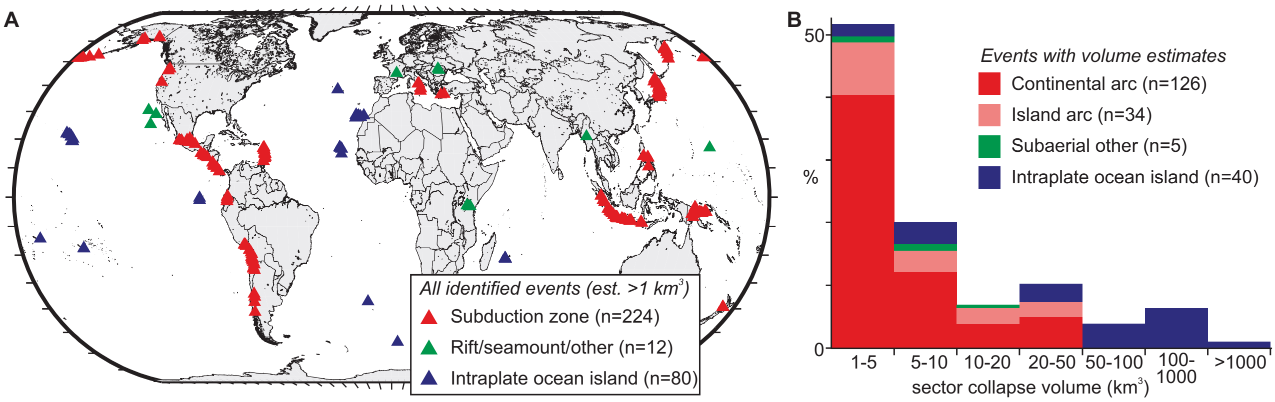
A
All identified events (est. >1 km^3)
Subduction zone (n=224)
Rift/seamount/other (n=12)
Intraplate ocean island (n=80)
B
50
%
0
Events with volume estimates
Continental arc (n=126)
Island arc (n=34)
Subaerial other (n=5)
Intraplate ocean island (n=40)
1-5
5-10
10-20
20-50
50-100
100-1000
>1000
sector collapse volume (km^3)

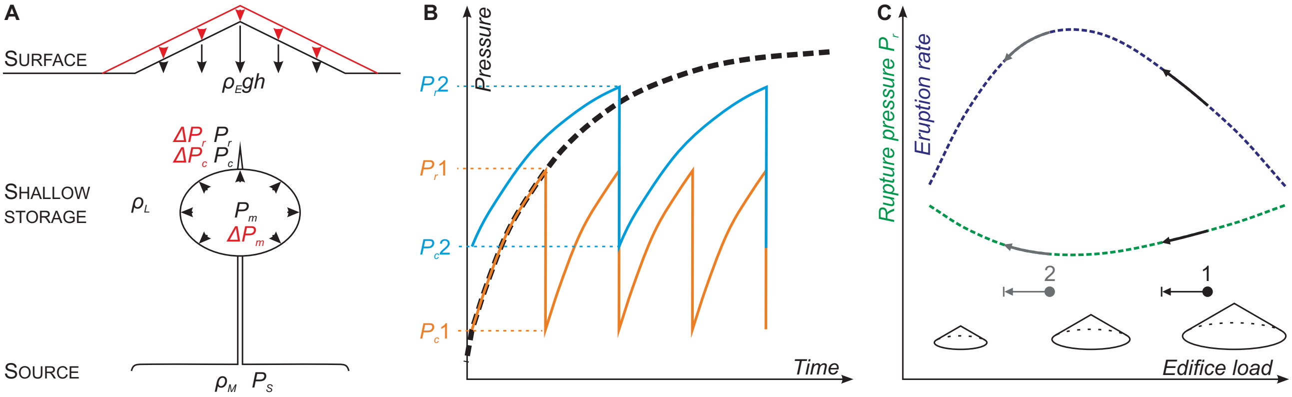

A
SURFACE
ρEgh
ΔPr Pr
ΔPc Pc
SHALLOW STORAGE
ρL
Pm
ΔPm
SOURCE
ρM PS
B
Pressure
Pr2
Pr1
Pc2
Pc1
Time
C
Rupture pressure Pr
Eruption rate
2
1
Edifice load

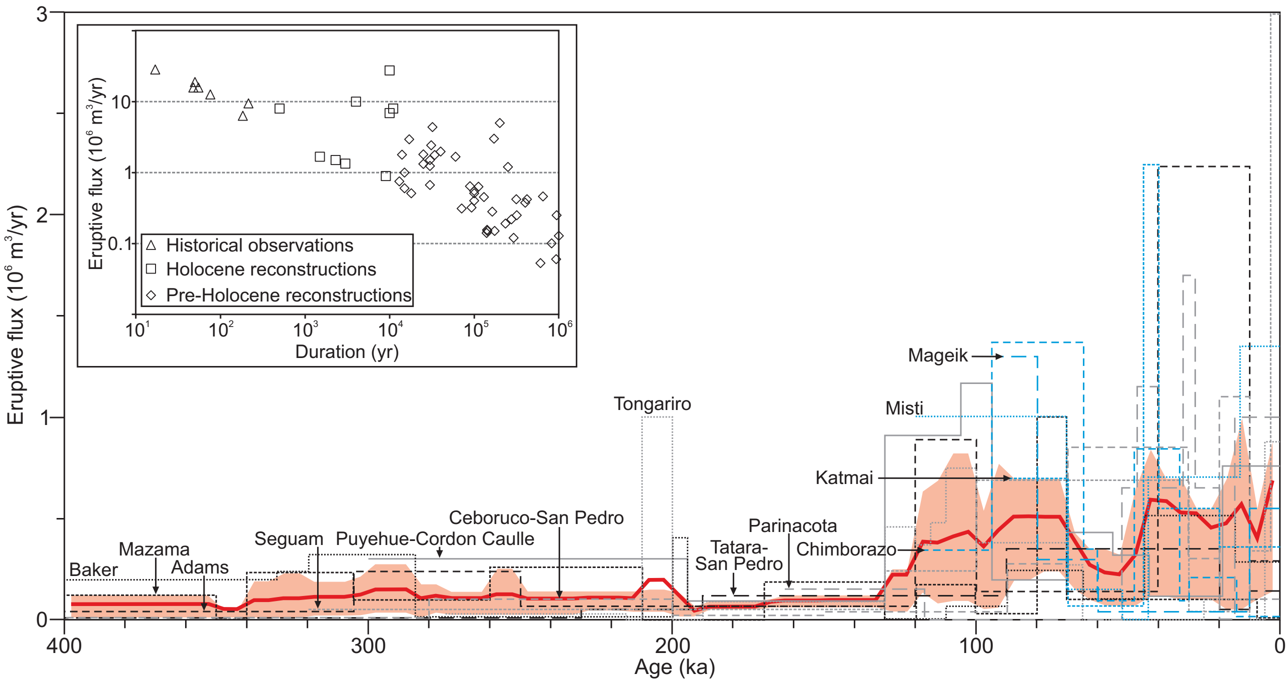

Eruptive flux (10^6 m^3/yr)
Age (ka)
Duration (yr)
Historical observations
Holocene reconstructions
Pre-Holocene reconstructions
Mageik
Misti
Katmai
Tongariro
Ceboruco-San Pedro
Puyehue-Cordon Caulle
Seguam
Mazama
Adams
Baker
Parinacota
Tatara-San Pedro
Chimborazo

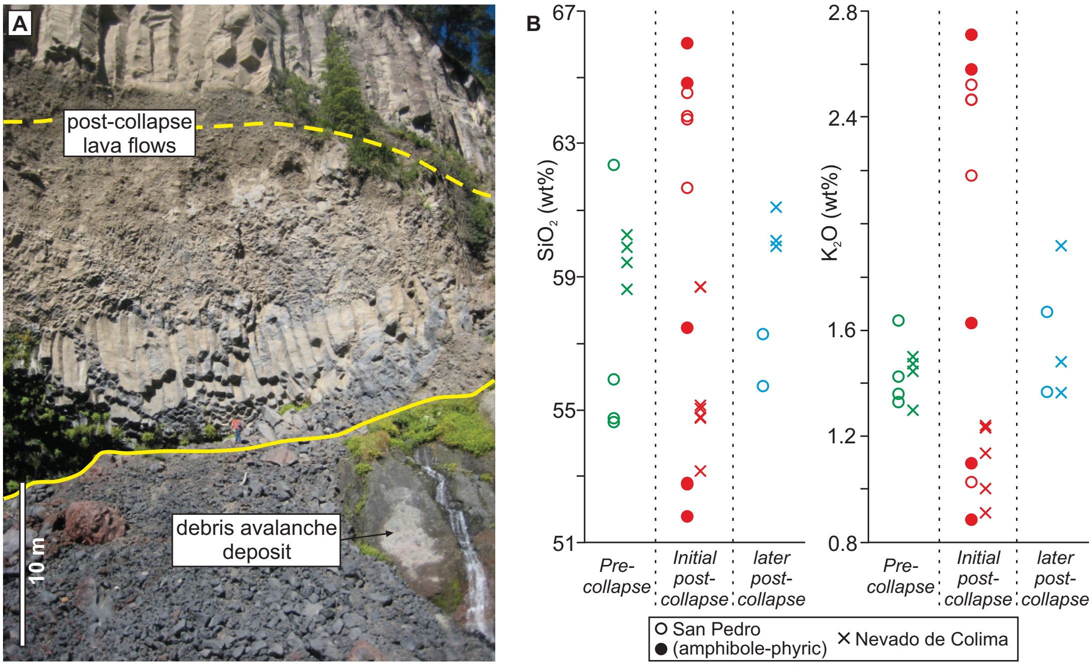
A
post-collapse
lava flows
debris avalanche
deposit
10 m
B
SiO2 (wt%)
67
63
59
55
51
K2O (wt%)
2.8
2.4
1.6
1.2
0.8
Pre-
collapse
Initial
post-
collapse
later
post-
collapse
San Pedro
(amphibole-phyric)
Nevado de Colima

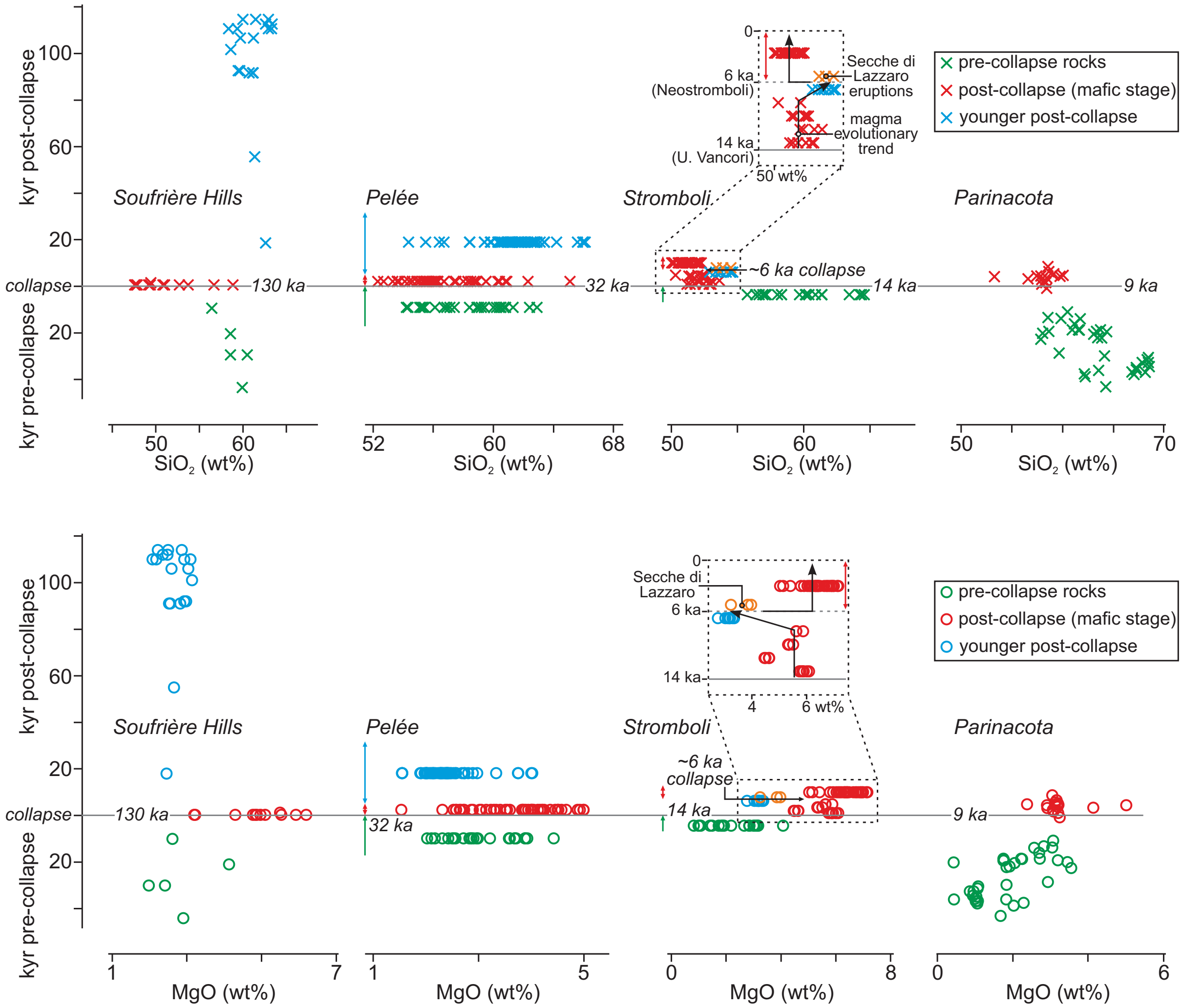

kyr post-collapse
kyr pre-collapse
collapse
100
60
20
20
Soufrière Hills
130 ka
SiO2 (wt%)
50
60
Pelée
32 ka
52
60
68
SiO2 (wt%)
Stromboli
~6 ka collapse
14 ka
50
60
SiO2 (wt%)
0
6 ka
(Neostromboli)
14 ka
(U. Vancori)
50 wt%
Secche di Lazzaro eruptions
magma evolutionary trend
Parinacota
9 ka
50
70
SiO2 (wt%)
pre-collapse rocks
post-collapse (mafic stage)
younger post-collapse
kyr post-collapse
kyr pre-collapse
collapse
100
60
20
20
Soufrière Hills
130 ka
1
7
MgO (wt%)
Pelée
32 ka
1
5
MgO (wt%)
Stromboli
~6 ka collapse
14 ka
0
8
MgO (wt%)
0
Secche di Lazzaro
6 ka
14 ka
4
6 wt%
Parinacota
9 ka
0
6
MgO (wt%)
pre-collapse rocks
post-collapse (mafic stage)
younger post-collapse

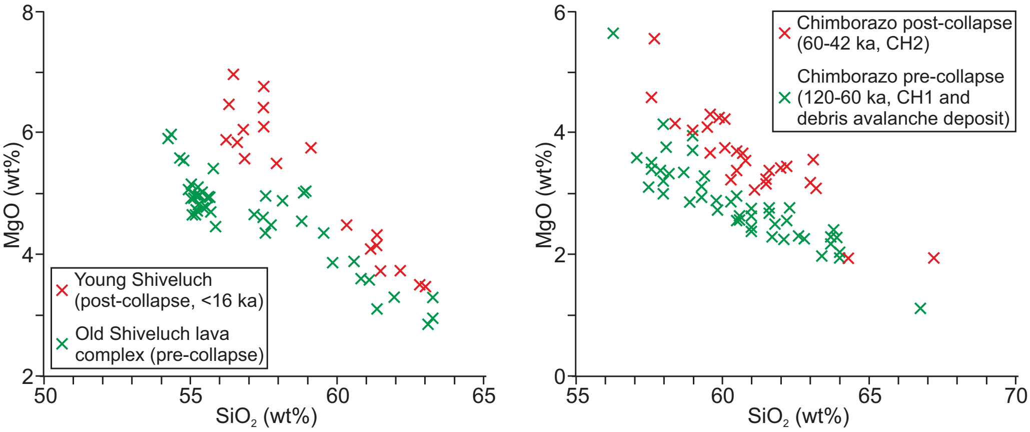

MgO (wt%)
SiO2 (wt%)
Young Shiveluch (post-collapse, <16 ka)
Old Shiveluch lava complex (pre-collapse)
Chimborazo post-collapse (60-42 ka, CH2)
Chimborazo pre-collapse (120-60 ka, CH1 and debris avalanche deposit)

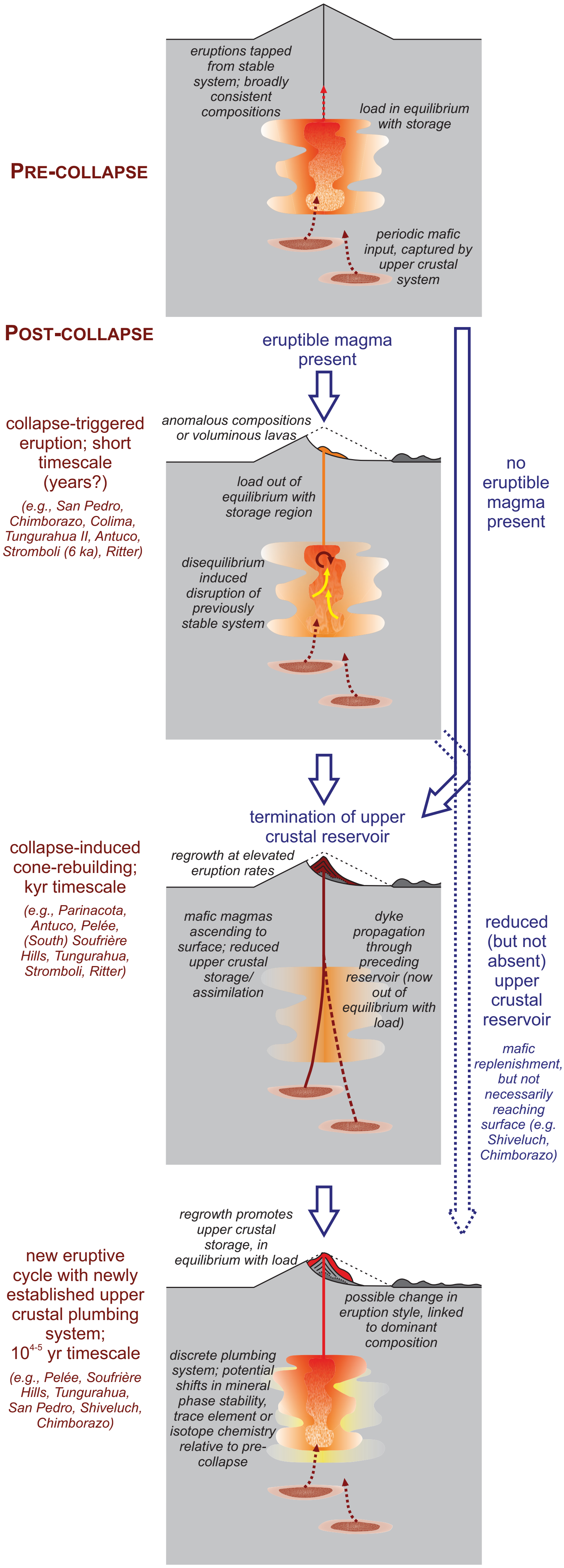

PRE-COLLAPSE
eruptions tapped from stable system; broadly consistent compositions
load in equilibrium with storage
periodic mafic input, captured by upper crustal system
POST-COLLAPSE
eruptible magma present
no eruptible magma present
collapse-triggered eruption; short timescale (years?)
(e.g., San Pedro, Chimborazo, Colima, Tungurahua II, Antuco, Stromboli (6 ka), Ritter)
anomalous compositions or voluminous lavas
load out of equilibrium with storage region
disequilibrium induced disruption of previously stable system
termination of upper crustal reservoir
collapse-induced cone-rebuilding; kyr timescale
(e.g., Parinacota, Antuco, Pelée, (South) Soufrière Hills, Tungurahua, Stromboli, Ritter)
regrowth at elevated eruption rates
mafic magmas ascending to surface; reduced upper crustal storage/ assimilation
dyke propagation through preceding reservoir (now out of equilibrium with load)
reduced (but not absent) upper crustal reservoir
mafic replenishment, but not necessarily reaching surface (e.g. Shiveluch, Chimborazo)
new eruptive cycle with newly established upper crustal plumbing system; 10^{4-5} yr timescale
(e.g., Pelée, Soufrière Hills, Tungurahua, San Pedro, Shiveluch, Chimborazo)
regrowth promotes upper crustal storage, in equilibrium with load
possible change in eruption style, linked to dominant composition
discrete plumbing system; potential shifts in mineral phase stability, trace element or isotope chemistry relative to pre-collapse

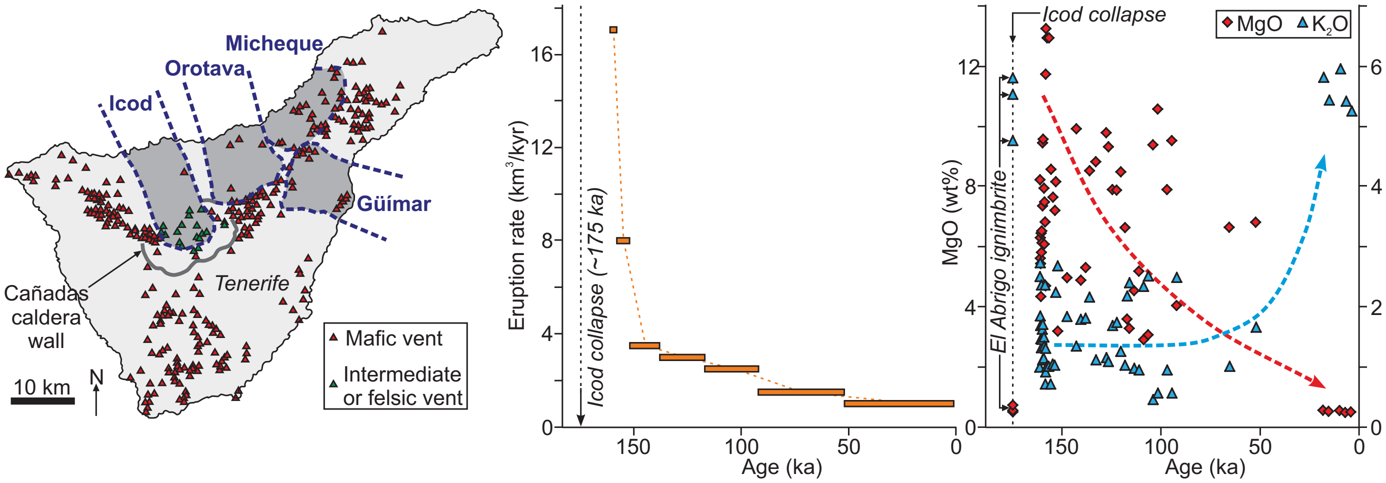
Micheque
Orotava
Icod
Güímar
Cañadas caldera wall
Tenerife
10 km
N
Mafic vent
Intermediate or felsic vent
Eruption rate (km³/kyr)
Icod collapse (~175 ka)
Age (ka)
Icod collapse
MgO
K₂O
MgO (wt%)
K₂O (wt%)
El Abrigo ignimbrite
Age (ka)

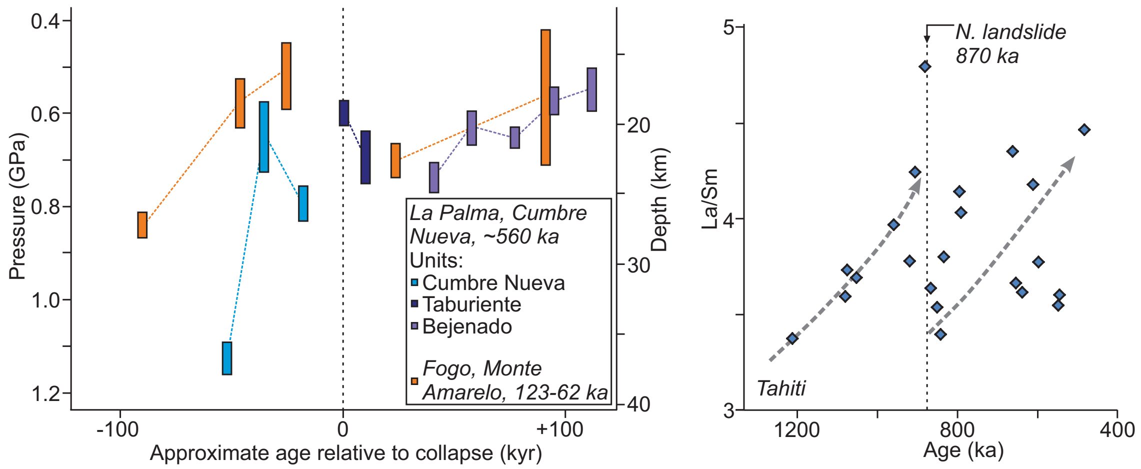
Pressure (GPa)
0.4
0.6
0.8
1.0
1.2
Depth (km)
20
30
40
-100
0
+100
Approximate age relative to collapse (kyr)
La Palma, Cumbre Nueva, ~560 ka
Units:
Cumbre Nueva
Taburiente
Bejenado
Fogo, Monte Amarelo, 123-62 ka
La/Sm
5
4
3
N. landslide 870 ka
Tahiti
1200
800
400
Age (ka)